

1   **EPIDURAL ELECTRICAL STIMULATION OF THE CERVICAL DORSAL ROOTS RESTORES**  
2   **VOLUNTARY UPPER LIMB CONTROL IN PARALYZED MONKEYS**

3   Beatrice Barra<sup>1,2,\*</sup>, Sara Conti<sup>1,\*</sup>, Matthew G. Perich<sup>3</sup>, Katie Zhuang<sup>1</sup>, Giuseppe Schiavone<sup>4</sup>,  
4   Florian Fallegger<sup>4</sup>, Katia Galan<sup>5,7</sup>, Nicholas D. James<sup>5</sup>, Quentin Barraud<sup>5,7</sup>, Maude Delacombaz<sup>1,7</sup>,  
5   Mélanie Kaeser<sup>1</sup>, Eric M. Rouiller<sup>1</sup>, Tomislav Milekovic<sup>3,7</sup>, Stephanie Lacour<sup>4</sup>, Jocelyne Bloch<sup>6,7</sup>,  
6   Grégoire Courtine<sup>5,6,7</sup> and Marco Capogrosso<sup>1,2,8</sup>

7   <sup>1</sup>Platform of Translational Neuroscience, Department of Neuroscience and Movement Sciences, Faculty of Sciences and Medicine,  
8   University of Fribourg, Fribourg, Switzerland

9   <sup>2</sup>Rehab and Neural Engineering Labs, University of Pittsburgh, Pittsburgh, USA.

10   <sup>3</sup>Department of Fundamental Neuroscience, Faculty of Medicine, University of Geneva, Geneva, Switzerland

11   <sup>4</sup>Bertarelli Foundation Chair in Neuroprosthetic Technology, Laboratory for Soft Bioelectronic Interfaces, Institute of  
12   Microengineering, Institute of Bioengineering, Centre for Neuroprosthetics, École Polytechnique Fédérale de Lausanne, Geneva,  
13   Switzerland.

14   <sup>5</sup>Center for Neuroprosthetics and Brain Mind Institute, School of Life Sciences, Ecole Polytechnique Fédérale de Lausanne,  
15   Lausanne, Switzerland.

16   <sup>6</sup>Department of Neurosurgery, CHUV, Lausanne, Switzerland;

17   <sup>7</sup>Defitech Center for Interventional Neurotherapies (NeuroRestore), University Hospital Lausanne (CHUV), University of Lausanne  
18   (UNIL) and Ecole Polytechnique Fédérale de Lausanne, Lausanne, Switzerland.

19   <sup>8</sup>Department of Neurological Surgery, University of Pittsburgh, Pittsburgh, USA

20   \*these authors contributed equally to this work

21   Correspondence to: Marco Capogrosso - mcapo@pitt.edu

22

23

24

25   **ABSTRACT**

26   Regaining arm control is a top priority for people with paralysis. Unfortunately, the complexity of  
27   the neural mechanisms underlying arm control has limited the effectiveness of neurotechnology  
28   approaches. Here, we exploited the neural function of surviving spinal circuits to restore voluntary  
29   arm and hand control in three monkeys with spinal cord injury, using spinal cord stimulation. Our  
30   neural interface leverages the functional organization of the dorsal roots to convey artificial  
31   excitation via electrical stimulation to relevant spinal segments at appropriate movement phases.  
32   Stimulation bursts targeting specific spinal segments produced sustained arm movements,  
33   enabling monkeys with arm paralysis to perform an unconstrained reach-and-grasp task.  
34   Stimulation specifically improved strength, task performances and movement quality.  
35   Electrophysiology suggested that residual descending inputs were necessary to produce  
36   coordinated movements. The efficacy and reliability of our approach hold realistic promises of  
37   clinical translation.

38

39 **MAIN TEXT**

40 **INTRODUCTION**

41 More than 5 million people in the US currently live with some form of motor paralysis<sup>1</sup>. Stroke and  
42 spinal cord injury (SCI) are the main causes with hundreds of thousands of new cases per year<sup>2</sup>.  
43 Impairments of the hand and arm are particularly problematic, representing a major unmet need  
44 for both SCI and stroke patient populations<sup>3,4</sup>. Indeed, even mild deficits in hand function lead to  
45 significant degradation of quality of life. Unfortunately, recovery of hand and arm motor function  
46 is still an unsolved clinical challenge.

47 Generated in the cerebral cortex, upper limb motor commands are relayed to subcortical and  
48 spinal circuits that activate motoneurons and regulate sensory inputs to produce skilled motor  
49 actions<sup>5–7</sup>. Spinal cord injury (SCI), or stroke, damage these communication pathways generating  
50 impairments in sensory regulation and motor functions that lead to motor paralysis.

51 Historically, neurotechnologies were conceived around the idea of restoring movements in  
52 paralyzed subjects via a technological bypass. Such solution would use signals from cortical  
53 areas as inputs and artificially compensate for lack of motoneuron activation by producing desired  
54 muscle activity below the lesion<sup>8</sup>. For example, both intraspinal micro stimulation<sup>9–11</sup> (ISMS) and  
55 functional electrical stimulation<sup>12</sup> (FES) were used to activate arm muscles in response to  
56 intracortical neural activity from the motor cortex. While ISMS was never attempted in human  
57 subjects, brain-controlled FES allowed paralyzed humans to perform voluntary grasping tasks<sup>13,14</sup>.  
58 However, translation of these concepts into daily clinical practice is hindered by two distinct  
59 limitations. First, the artificial motoneuron recruitment order generated by FES induces muscle  
60 fatigue<sup>15</sup> which is particularly problematic for arm movements. Indeed, fatigue prevents the  
61 generation of sustained forces and consequently FES fails to enable sustained three-dimensional  
62 arm movements that are required for daily activities. Second, since FES bypasses surviving  
63 circuits in the spinal cord, complex stimulation protocols and sophisticated decoding algorithms<sup>1</sup>  
64 are required to orchestrate the activation of multiple muscles and produce functional movements.  
65 As a result, these systems require an articulated combination of hardware and software.  
66 Unfortunately, this complexity does not cope well with dynamic clinical environments that need  
67 robust and practical solutions for a rapid set up and large-scale use.

68 In contrast, epidural electrical stimulation (EES) of the lumbar spinal cord exploits surviving spinal  
69 circuits and supra-spinal connections after injury to produce movements<sup>16</sup>. Similar to intraspinal  
70 stimulation<sup>11,17</sup>, EES engages motoneurons via direct recruitment of large sensory afferents<sup>18</sup>  
71 leading to widespread excitatory post-synaptic potentials in the spinal cord. More importantly,  
72 since motoneurons are recruited via natural synaptic inputs, EES generates a natural recruitment  
73 order<sup>19</sup> that is resistant to artificial fatigue. This enables the production of forces that can sustain  
74 the whole-body weight<sup>20</sup>. Moreover, engagement of motoneurons from pre-synaptic pathways  
75 allows residual descending inputs and spinal circuits to control motoneurons excitability and  
76 produce voluntary movement after complete motor paralysis<sup>21</sup>.

77 Building on animal models<sup>22–24</sup>, recent clinical studies have shown that continuous stimulation  
78 delivered through epidural implants on the dorsal aspect of the lumbosacral spinal cord increased  
79 muscle strength, voluntary muscle activation and single joint movements in people with complete  
80 leg paralysis<sup>21,25</sup>. More strikingly, when coupled with targeted physical rehabilitation protocols,  
81 continuous EES restored weight bearing locomotion in subjects with severe SCI<sup>26,27</sup>. These  
82 outstanding clinical results prompted experimental studies aiming at verifying whether EES could  
83 be used to promote also upper limb movements after SCI<sup>28</sup>. Unfortunately, while clinical studies

87 showed some success in improving hand grip force with both epidural and non-invasive  
88 approaches<sup>29,30</sup>, continuous EES did not produce results of similar outstanding efficacy as those  
89 observed for the lower limbs<sup>26,27</sup>. In fact, clinical outcomes were similar to those obtained with  
90 surface FES<sup>31</sup>.

91 Reasons for this discrepancy may stem from the complexity of upper limb motor control and  
92 biomechanics compared to locomotion. Indeed, in contrast to pattern-driven<sup>32</sup> and repetitive  
93 locomotor movements, upper limb movements are composed by a non-repetitive and task-  
94 dependent combination of movement modules which are highly dependent from sophisticated  
95 cortico-spinal control<sup>6,33-35</sup> and accurate sensory feedback<sup>36,37</sup>. Because of this intrinsic  
96 complexity, non-specific neuromodulation could limit the efficacy of EES by exciting all spinal  
97 segments simultaneously, irrespectively of movement phase. More importantly, unspecific and  
98 continuous stimulation of the sensory afferents through EES disrupts natural sensory inputs<sup>19</sup>  
99 thus hindering spinal regulation of movements which is critical in dexterous upper limb control<sup>36,37</sup>.  
100 We and others have shown that it is possible to direct electrical stimulation of the spinal cord to  
101 target restricted segments during appropriate times<sup>17,38</sup>. These spatio-temporal stimulation  
102 protocols enabled voluntary locomotion in monkeys with SCI as early as day 6 post injury without  
103 any physical training<sup>39</sup> and within 2 weeks post implantation in humans with complete leg  
104 paralysis<sup>20</sup>. This approach exploits the somato-topography of the spinal sensory system to  
105 selectively engage restricted spinal regions<sup>18,38</sup>. Unfortunately, non-invasive technologies and  
106 clinically approved electrodes are unfit for this scope<sup>40</sup> because of their limits in selectivity.  
107 Therefore, we hypothesized that a neural interface, specifically designed to target the cervical  
108 dorsal roots, could enable the administration of spatio-temporal stimulation patterns to the cervical  
109 spinal cord. We tested this hypothesis in three monkeys with a unilateral cervical SCI. We  
110 designed a personalized epidural interface to target primary afferents within the cervical dorsal  
111 roots. We hypothesized that the electrical stimulation of the roots with bursts linked to movement  
112 attempts would enable voluntary motor control and improve functional deficits of the arm and hand  
113 that emerge after SCI. Specifically we tested for improvements in muscle strength, dexterity and  
114 ability to execute three-dimensional functional tasks in full independence. Finally, we verified that  
115 the mechanisms enabling the voluntary recruitment of motoneurons in the cervical spinal cord  
116 were similar to those occurring during EES of the lumbosacral circuits.

117

## 118 **Results**

119

### 120 **Natural arm movements**

121 Clinically effective systems should enable truly functional arm movements rather than simplified  
122 tasks such as single-joint movements. A functional arm movement entails a coordinated activation  
123 of arm muscles to achieve a desired movement while supporting the arm weight at all times. Most  
124 of daily activities require arm extension (reach) and flexion (pull), combined with a hand-grasp  
125 without a constrained timing or structure. Consequently, we developed a robotic platform allowing  
126 the quantification of reach, grasp and pull movements<sup>41</sup> that would feel natural and unconstrained  
127 to monkeys both in trajectory and timings (**Figure 1A**). We trained three adult *Macaca fascicularis*  
128 monkeys to reach for, grasp, and pull an instrumented object placed on the end effector of our  
129 robotic arm (**Figure 1B**). Movement trajectories were not constrained neither kinematically nor in  
130 time. Monkeys waited for the go signal, reached for the object and pulled to receive a food or juice  
131 reward when the object crossed a pre-defined displacement threshold<sup>41</sup>. Monkeys intuitively and  
132 rapidly learned this task by developing their own individual kinematic strategies (**Extended Data**  
133 **Figure 1**) and personal movement speeds. We then designed a battery of electrophysiology and  
134 kinematic measurements to evaluate functional outcomes on task performances, muscle  
135 activation, muscle strength and movement dexterity. Specifically, we quantified full-limb 3D

136 kinematics (Vicon Motion Systems, Oxford, UK), pulling forces, and electromyographic (EMG)  
137 signals from intramuscular leads in eight arm muscles (**Figure 1A, Extended Data Figure 1**).  
138 Before SCI, we observed clear bursts of EMG activity from all hand and arm muscles during the  
139 three movement phases: reach, grasp, and pull in all monkeys. Finally, to document the  
140 involvement of cortical neurons during movement enabled by EES and to extract signals that  
141 could also be used to link stimulation bursts to movement phase onset, we implanted multi-  
142 microelectrode arrays (Blackrock Microsystems, Salt Lake City, USA) in the arm/hand region of  
143 the right sensorimotor (M1, S1) and ventral premotor (PMv) cortex. We validated these recordings  
144 by verifying that neural activity was consistently modulated with kinematics pre-injury and with the  
145 three movement phases as largely expected<sup>41</sup> (**Figure 1, Extended Data Figure 1**). In summary,  
146 we analyzed natural arm movements in monkeys and concluded that in order for stimulation  
147 protocols to be effective, it was important to support reach, grasp and pull independently with  
148 specific parameters for each animal.  
149  
150

### 151 **Personalized spinal interface**

152 To design an optimal interface, we studied the anatomy of the monkey cervical spinal cord. We  
153 extrapolated available anatomical information from literature and found that, similar to humans,  
154 motoneurons innervating arm muscles in the monkeys are segmentally organized<sup>40</sup> (**Figure 1C**).  
155 We previously showed that stimulation of a single cervical dorsal root will recruit motoneurons  
156 that receive direct afferent inputs from that root<sup>40</sup>. Exploiting this property allows to obtain a  
157 segmental recruitment order of motoneurons that can be targeted to promote specific movement  
158 phases<sup>20,38,42</sup>. Therefore, we designed a spinal interface that could target each root independently.  
159 We achieved this by placing contacts on the lateral aspect of the cord to target the entry zone of  
160 each individual root<sup>40</sup>. Since each monkey displayed a unique anatomy, we tailored the design of  
161 our interface to each specific subject. For this, we measured white matter diameter and vertebral  
162 canal features from computed tomography (CT) and magnetic resonance imaging (MRI). We then  
163 spaced the electrodes rostro-caudally and medio-laterally to match the transversal and  
164 longitudinal dimensions of the cord of each animal (**Extended Data Figure 2A, 2B**). This allowed  
165 us to simplify the neural interface architecture by minimizing the number of contacts while  
166 maintaining high muscle recruitment specificity<sup>43</sup>. We then designed a surgical strategy to position  
167 the epidural interface between the C6 and T1 dorsal roots (**Figure 1D**). We performed  
168 laminectomies between the T1 and T2 vertebrae and the C5 and C6 vertebrae, then pulled the  
169 neural interface through the intermediate epidural space with the help of a custom soft inserter<sup>43</sup>.  
170 We verified that the position of the array remained stable for the entire duration of the study (up  
171 to 3 weeks) through repeated X-ray imaging (**Figure 1D, Extended Data Figure 2C**). During the  
172 same surgery, we performed a unilateral spinal cord injury at the C5/C6 segments (**Figure 1E**)  
173 aiming at transecting the cortico-spinal tract that is located on the lateral aspect of the white matter  
174 in monkeys. This type of lesion is amply described in literature and induces unilateral arm and  
175 hand paralysis<sup>1</sup> while preserving important bodily functions such as bladder control. Postmortem  
176 immunohistochemistry analysis of the spinal cords showed that the spinal interface did not  
177 damage the cervical cord in any of the three monkeys but did reveal that Mk-Br received an  
178 unplanned compression injury at the insertion site (T3 spinal segment). Given the caudal position  
179 of this contusion it is likely for it to have occurred during implantation (**Extended Data Figure 2D**).  
180 Since the T3 segment is below the innervation of the arm motoneurons, this lesion did not affect  
181 the phenotype of arm and hand motor deficits which did not differ from the other monkeys (see  
182 Methods).

183 In summary, we designed a spinal interface to selectively recruit the cervical dorsal roots. We  
184 tailored the interface to the specific anatomy of each monkey and designed a surgical strategy to  
185 perform a consistent and stable implantation.

186

### 187 **EES can produce functional movements and grasp**

188 We next assessed the selectivity of the epidural interface. In propofol anaesthetized monkeys, we  
189 delivered asymmetric, charge-balanced biphasic pulses of EES at low repetition rate (1Hz) at  
190 various current amplitudes from each contact. Minimum and maximum amplitude values were  
191 selected as the first subthreshold and first saturation current value respectively. As predicted<sup>40</sup>,  
192 different stimulation contacts generated muscle recruitment patterns that mirrored the segmental  
193 organization of cervical motoneurons (**Figure 2A, Extended Data Figure 3**). Specifically,  
194 contacts located at C8/T1 level (caudal) elicited spinal reflexes mostly in the hand and forearm  
195 muscles, contacts located at C7 level elicited triceps and contacts located at C5/C6 recruited  
196 biceps and deltoids (rostral). Those results were consistent in all animals (**Figure 2B, Extended**  
197 **Data Figure 3**). To ensure that this segmental selectivity translated into separate functional arm  
198 and hand movements, we delivered supra-threshold stimulation at various frequencies (20-120  
199 Hz) from each contact in two animals (Mk-Br and Mk-Yg). Indeed, since recruitment of  
200 motoneuron is pre-synaptic, EES may not be able to produce sustained muscle activation  
201 because of frequency dependent suppression<sup>46</sup>. This effect is an observed substantial  
202 suppression of muscle evoked potentials during repetitive stimulation of the afferents. Instead, we  
203 observed large and sustained arm movements during EES bursts. Muscle selectivity was  
204 preserved during long stimulation trains (**Figure 3C, F**) and different contacts elicited distinct  
205 functional joint movements (**Figure 3A, B, D, E, Video 1**) such as shoulder abduction, elbow  
206 extension and whole hand grasp. When looking at the energy of the EMGs, we found a monotonic  
207 relationship between muscle activation and stimulation frequency in most of the upper arm  
208 muscles (**Figure 3C, F**). However, not all muscles showed such clear frequency dependent  
209 responses (**Extended Data Figure 4A**). Moreover, peak-to-peak responses (**Extended Data**  
210 **Figure 4B**) were generally decreased during a burst at high frequency but were not abolished  
211 and tended to vary during the burst and while the movement was produced. We used these  
212 observations to optimize stimulation parameters to be used in a behavioral reach and grasp task  
213 (see Methods and **Extended Data Figure 5**). In summary, we found that single contacts of our  
214 spinal interface elicited segmental recruitment of arm flexors, extensors and hand flexors. Bursts  
215 of stimulation from these contacts produced sustained joint movements that were graded by  
216 stimulation frequency (**Extended Data Figure 6**).

217

218

219

### 220 **EES improves arm and hand function after spinal cord injury**

221 We next tested whether our stimulation protocol could improve functional outcomes of upper limb  
222 movements after SCI. Specifically, we tested the efficacy of EES to improve muscle activation,  
223 pulling forces, functional task performance, and kinematic quality of three-dimensional  
224 movements after SCI when stimulation was on against stimulation off as a control. In all monkeys,  
225 the lesion led to substantial motor deficits of the left arm and hand.

226 While each monkey retained the ability to activate proximal shoulder and biceps muscles, elbow  
227 extension and hand functions were severely compromised. Severity of the impairment and extent  
228 of spontaneous recovery (**Extended Data Figure 7**) varied across monkeys because of the  
229 variability in lesion size (**Figure 1E**). Generally, animals showed severe paralysis immediately  
230 after lesion, and then gradually regained some movement capabilities (**Extended Data Figure 7**).  
231 Due to the initial impairment, immediately after the lesion, monkeys were not able to perform the

behavioral task. Consequently, during the first week, we simplified the task by presenting an object close to the monkeys and triggering stimulation bursts manually to encourage the animal to perform the task. After the first week, all monkeys spontaneously attempted to perform the task, making it possible to link the delivery of movement-specific stimulation bursts to real-time detection of movement onset using intra-cortical signals. Whenever the monkeys strived for a reach, grasp or pull movement, we delivered bursts of stimulation promoting reach or grasp/pull respectively (movement specific EES). Outcomes were computed for each animal independently and compared between EES on and EES off. In terms of functional task performances, without stimulation Mk-Br and Mk-Yg were more capable of completing reach movements than grasp and pull, which is consistent with their lesion severity. Stimulation improved overall movement performances but differentially according to specific animal's deficits. We found that the majority of times that a monkey had completed a portion of the task it had done so during EES (**Figure 4B**). More specifically, Mk-Sa suffered the most severe deficits and could only reach during EES and never without (**Figure 4B**). Similarly, Mk-Yg was never able to grasp or pull without EES, whereas Mk-Br could perform only a handful of grasps and pulls without stimulation. Interestingly, performance changed overtime. For example, in both Mk-Br and Mk-Yg improvements in grasps and pull emerged only later when the animals spontaneously recovered some movement capacity (**Figure 4B, Video 2,3,4**). More specifically Mk-Br improved grasp and pull only after 2 weeks with stimulation while Mk-Yg could grasp with stimulation by the end of week 1 (**Figure 4B**) which was unfortunately the last day we could test this task because the grasp contact E6 failed after (see Methods). Instead, when we used our interface to deliver continuous EES that was not related to movement onsets, only non-significant and modest improvements were observed in Mk-Br while Mk-Yg did not show ability to grasp and pull during continuous EES (**Extended Data Figure 8A**). Moreover, we analyzed trials in which stimulation bursts were not triggered at movement onset, for example when pull stimulation was erroneously triggered during reach. In these trials the reach movement was abruptly interrupted, and the animal did not complete the task (**Extended Data Figure 8B, Video 5**).

During phase dependent stimulation, EES enhanced muscles activity and forces (**Figure 5A,B**) compared to no stimulation. In terms of movement quality, EES bursts triggered at movement onset significantly improved the overall quality of arm movements (**Figure 5B**). Indeed, principal component analysis (PCA) of three-dimensional kinematic parameters (i.e., timing, force, arm trajectories, joint angles) revealed that during EES, movement kinematics were significantly closer to pre-lesion kinematics than the few successful movements performed without stimulation (distance from pre-lesion performances in the multi-parametric kinematic space, **Figure 5B**). Notably, animals sustained the weight of the arm and lifted their elbow more, performed wider movements, and generated stronger forces (**Figure 5B**), getting closer to normal kinematic trajectory patterns without any long-term training.

In summary, we showed that EES bursts triggered at movement phase onsets, improved muscle strength, task performance and quality of arm movements. This allowed monkeys to perform reach, grasp and pull movements that were otherwise not able to perform without EES.

#### **Sensory inputs can decrease EES-induced motor output**

We then investigated the role of spinal circuits and sensory inputs in the production of the movements that we observed. Indeed, since activation of motoneurons was pre-synaptic, spinal reflexes and sensory inputs can influence EES evoked spinal reflexes in the legs<sup>38</sup>. In order to exclude influences of residual supraspinal voluntary inputs, we conducted experiments under propofol anesthesia (**Figure 6A**) with Mk-Br. We then delivered bursts of EES from the contact eliciting elbow flexion at varying stimulation frequencies in two distinct conditions (**Figure 6B**): in

isometric and unconstrained conditions. In the isometric condition, we constrained the wrist, elbow and shoulder of the animal and measured force production at the wrist joint. Under unconstrained conditions we left the arm free to move under the effect of stimulation. This setup only differs from the sensory feedback generated at the load when pull forces are produced by EES. We found that EES induced EMG activity during unconstrained movement that was significantly different from the EMG activity induced during isometric movements (**Figure 6B**). In particular, overall EMGs and peak-to-peak amplitudes of elicited spinal reflexes were significantly lower when the arm was attached to a load (isometric) compared to when it was free to move. Albeit present at all frequencies, this difference was particularly important within the 40 to 60Hz range, thus overlapping with the functional frequency ranged that we selected for our study. These results show that force loads at the hand decreased EMG activity induced by EES as compared to no load applied at the hand. Under anesthesia, only changes on spinal circuit excitability induced by sensory inputs can explain the observed changes on EES evoked muscle activity.

## Residual cortical input is necessary

The influence of spinal sensory inputs showed that EES output may be decreased because of spinal sensory inputs when loads are applied at the hand. This would decrease the efficacy of EES which is supposed to enhance force production. Therefore, to explain the results we obtained in behaving monkeys (**Figure 6**) we investigated the contribution of residual cortical inputs in the production of forces and movements during EES. Specifically, since cortical inputs actively modulate spinal circuits, they should be able to both enhance and suppress EES output by modulating spinal circuit excitability<sup>21</sup>. Since we showed that monkeys could use EES to amplify their movement and forces (**Figure 6D**) we focused on demonstrating that cortical inputs could also suppress unwanted EES-generated movements. We hypothesized that if monkeys did not want to move, EES would not produce the large joint movements that we observed when the monkeys were anesthetized. Therefore, we identified trials in which our decoder detected a false-positive reach movement (**Figure 6C**). In this situation our system would deliver a burst of stimulation even if the animal was not attempting to execute the task. We then compared intracortical activity from the primary motor cortex (M1) of Mk-Br and Mk-Yg during these false-positive trials to the signals recorded during correctly detected trials. We identified trials where EES was present and the monkey moved, and trials when EES was present but the monkey did not move (**Figure 6D**). We verified that the same neural units were present in both conditions and found that the overall firing rates of all units in motor cortex was significantly higher when EES produced movement (**Figure 6E**) than when it did not. This suggested that movement happened only if the motor cortex was active, despite EES was delivered at amplitudes that generated large joint movements when the same monkey was anesthetized. To further validate this hypothesis we applied dimensionality reduction using Principal Component Analysis to the firing rates in each electrode and reduced the M1 population activity to low-dimensional states<sup>47</sup>. In this low-dimensional space each point represents the global neural state of the motor cortex at a given time point (**Figure 6F**). We compared the neural states present when EES was associated movements and those when EES was not associated movement with the neural states associated to rest, e.g. when the monkeys were resting before the go signals between trial repetitions. When looking at the spatial distribution of neural states, trials in which EES was not associated to movement seemed to overlap with states of rest. We then computed the distance between each neural state to the subspace representing neural states at rest and found that the neural states associated to movements during EES were significantly further away from neural states at rest than neural states associated to EES and no movement. In summary, we found that the motor cortex activity was similar to the activity at rest whenever we delivered EES but the monkey did

330 not move (**Figure 6F**). Instead, the monkey moved when the motor cortex was significantly active.  
331 This implies that the residual cortical inputs via direct and indirect pathway can either suppress  
332 or enable movement during EES.

333  
334

### 335 **Discussion**

336 We showed that EES of cervical spinal cord immediately enhanced muscle activation and strength,  
337 task performances and movement quality during a natural-like reach and grasp task in monkeys  
338 with unilateral cervical SCI compared to no stimulation controls in three monkeys. Importantly,  
339 our technique allowed monkeys to support the weight of their arm during reach, grasp and pull  
340 movements. These results are important in light of clinical translation of our technology. Stronger  
341 forces and better arm weight bearing can empower patients with the capacity to perform a larger  
342 spectrum of movements than they would normally be capable of doing without the need of support.  
343 This may provide for more independence in daily living as well as better outcomes of physical  
344 therapy.

345

### 346 **Exploiting subject-specific anatomy to simplify technology**

347 We obtained our results with relatively simple stimulation protocols that engaged up to three  
348 monopolar contacts (one for reach, one for grasp and one for pull). The combination of simple  
349 bursts through these contacts enabled whole arm multi-joint movements. We believe that the  
350 design of our interface was key to achieve this result. The dorsal roots are a robust anatomical  
351 target that we could easily identify through standard imaging to personalize surgical planning and  
352 interface design. A similar surgical planning approach can be imagined in humans where MRIs  
353 and CT can guide surgical planning<sup>20</sup>.

354 Our results were enabled by the relative mapping between each dorsal root and the rostro-caudal  
355 distribution of motoneurons in the cervical spinal cord, which is similar in monkeys and humans<sup>40</sup>.  
356 The anatomical separation of roots in the cervical enlargement allowed us to recruit each root  
357 independently which generated distinct joint movements to a degree that was not observed in  
358 applications of EES for the lower limbs<sup>38</sup>. Stimulation of the C6 root elicited distinct arm flexion,  
359 C7 stimulation produced arm extension and C8/T1 stimulation produced hand grasp. However,  
360 similarly to other spinal cord stimulation studies we could not identify contacts that selectively  
361 produced finger extension<sup>11,48</sup>. This is likely caused by the overlap of extensor motor-pools in the  
362 forearm<sup>40</sup> but possibly also because flexors may be biomechanically stronger and dominate hand  
363 kinematics in the case of co-contraction at rest. Despite these limitations in specificity, we were  
364 able to restore a whole three-dimensional arm movement by solely detecting movement onset  
365 signals to trigger pre-determined stimulation bursts through two or three contacts. Unlike FES,  
366 this is possible because EES activates cervical motoneurons via pre-synaptic inputs thus allowing  
367 modulation of elicited muscle responses that can compensate for reduced specificity<sup>38</sup>.

368

### 369 **Supporting arm movement phases independently**

370 Contrary to previous pilot applications of epidural and transcutaneous spinal cord stimulation of  
371 the cervical spinal cord<sup>29,30</sup>, we utilized a soft epidural interface that allowed selective and  
372 independent support of each movement phase rather than providing continuous stimulation to the  
373 whole spinal cord. This approach is not possible with transcutaneous technologies<sup>49</sup> or current  
374 design of human leads<sup>40</sup> and would require new interfaces designed for the cervical cord.  
375 Selective spatiotemporal stimulation was shown to be more effective in animal models and  
376 humans than continuous stimulation in the sense that it was able to immediately produce  
377 coordinated locomotion compared to continuous stimulation that instead required long training  
378 periods<sup>23,38,42</sup>. In the case of the upper limb we believe that this approach was critical. Indeed,

379 while continuous stimulation did provide some level of facilitation, it failed to entirely promote  
380 grasp and pull in one of the monkeys. Perhaps the intrinsically unstructured nature of arm and  
381 hand control makes a continuous stimulation approach less effective than it is in locomotion that  
382 instead has an intrinsic repetitive structure<sup>32</sup>. For example, stimulation parameters that promote  
383 grasp, may impair reach if they are delivered continuously throughout movement. Indeed, when  
384 a pull stimulation was triggered at mid-reach it generated the interruption of the reach movement.  
385 Perhaps a different interface design or lower stimulation amplitudes could be used to optimize  
386 continuous stimulation protocols, but it would be at the expense of power of elicited movements  
387 potentially preventing the weight bearing component necessary for three-dimensional movements.  
388 In summary, the complex articulation of arm and hand movements may exacerbate the difference  
389 in efficacy between continuous and phase-specific stimulation protocols that was already  
390 observed for EES in locomotion, possibly explaining the difference in effect size that was obtained  
391 so far for application in the upper limb.

392

### 393 **The role of sensory feedback and residual cortical inputs**

394 We showed that sensory feedback when the hand was constrained to a force load reduced the  
395 EMG power produced by EES compared to free movements. This is likely caused by afferent  
396 inhibitory feedback coming from Ib afferents<sup>50</sup>. Unfortunately, lower muscle power while resisting  
397 a force load would decrease the clinical usability of this technology. We believe that this  
398 phenomenon is particularly relevant for the upper limb. Indeed, also during EES of the  
399 lumbosacral cord, the EES motor output is influenced by sensory inputs<sup>38</sup>, however sensory inputs  
400 are instrumental for locomotion and heavily contribute to the generation of the repetitive  
401 movement patterns that are required to walk<sup>16,19,32,51</sup>. Therefore, in the case of locomotion these  
402 inputs amplified and sustained EES-induced activity<sup>16,19,23</sup>. Instead arm and hand movements are  
403 produced by an unstructured sequence of primitive movements<sup>33</sup> and reflexes<sup>36</sup> in parallel with a  
404 sophisticated gating of sensory inputs through mechanisms such as pre-synaptic inhibition<sup>7</sup>.  
405 Therefore, residual cortical inputs become instrumental to obtain arm and hand movement with  
406 EES as shown by our analysis of intra-cortical signals during the production of movement  
407 combined with the observation that functional grasp was achieved only when the animals had  
408 recovered some level of function. Indeed, our lesions were non-complete and while most of the  
409 cortico-spinal tract was transected, multiple residual descending pathways were spared. These  
410 indirect inputs could have been used by the animals to mediate the inputs required to integrate  
411 EES and sensory inputs to produce voluntary movements. In summary, we believe that even  
412 during phase-specific EES residual cortical inputs play a critical role in enabling arm movement  
413 for cervical EES.

414

### 415 **Clinical significance and challenges**

416 The most important challenge for clinical translation of EES to humans concerns the role of  
417 residual inputs. Our data show that some level of residual inputs and of function is required to  
418 enable movement, first because in awake animals EES did not initiate movements, and second  
419 because it lacks the selectivity to achieve selective finger activity. However, previous studies  
420 showed that even completely paralyzed subjects retain residual but functionally silent descending  
421 inputs-. Therefore, while overall efficacy may depend on injury severity, even severely injured  
422 patients may obtain benefits from cervical EES. After a period of physical training combined with  
423 EES<sup>52</sup> these subjects may be able to use EES to achieve simple but functional grasp. Alternatively,  
424 more selective technologies targeting hand muscles such as FES could be combined with EES  
425 to obtain powerful yet selective movements.

426 The adaptation of EMG output to stimulation frequency that we observed in consequence of pre-  
427 synaptic activation of motoneurons may lead to a reduction in efficacy during long-term clinical

428 use. Additionally, stimulation of afferent fibers may cause uncontrolled reflexes which may affect  
429 function. While we did not observe these phenomena in our data, this may be due to the relatively  
430 small size of the lesion compared to severe contusion in humans. However, data in humans with  
431 SCI suggest that stimulation protocols can be adapted to be functional even in subjects with  
432 chronic severe thoracic lesions<sup>20,26</sup>, therefore we expect that this will be the case also for cervical  
433 lesions. At any rate both risks can be reduced by accurate stimulation tuning and real-time  
434 adaptation of stimulation patterns<sup>53</sup>.

435 Concerning complexity of our system, in our study we detected movement onsets from  
436 intracortical activity which may be seen as a limitation for a realistic implementation of our protocol  
437 in clinical settings. However, given the simplicity of our protocol which is essentially constituted  
438 by alternation of pre-defined bursts, brain recordings may not be required in clinics. Indeed, most  
439 patients suffer from a severe but incomplete paralysis<sup>20</sup>, which spares some residual muscle  
440 activity in few muscles. While this residual activity is not sufficient to produce functional  
441 movements, it can be reliably detected and used to trigger stimulation bursts with standard clinical  
442 technologies<sup>20,38</sup>. In summary, we believe that by exploiting the functionality of residual spinal  
443 circuits and supra-spinal inputs, cervical EES constitutes a simple yet robust approach to the  
444 restoration of arm motor control with significant translational potential.

445

#### **Acknowledgements**

446 The authors would like to thank Jacques Maillard and Laurent Bossy for the care provided to the  
447 animals, Dr Eric Schmidlin and Dr Simon Borgognon for their help with anaesthesia and surgery  
448 preparations, Dr Marion Badi for her help and advice during experiment preparations and  
449 experimental procedures, Dr. Andrina Zbinden for her contribution to the health survey of the  
450 monkeys, André Gaillard and Andrea Francovich for their help with the implementation of the  
451 hardware and the students of the University of Fribourg Amélie Jeanneret, Alen Jelusic, Laora  
452 Marie Jacquemet and Samia Borra for their help in processing data.

453

#### **Funding**

454 The authors would like to acknowledge the financial support from the Wyss Center grant (WCP  
455 008) to MC, GC and TM, an industrial grant from GTX medicals to GC and MC; the Bertarelli  
456 Foundation (Catalyst Fund Grant to MC and TM and funds to SL) a Swiss National Science  
457 Foundation Ambizione Fellowship (No. 167912 to MC), a Swiss National Science Foundation  
458 Doc-Mobility Grant (No. 188027 to BB), The European Union's Horizon 2020 research and  
459 innovation program under the Marie Skłodowska-Curie grant agreement no. 665667 (GS) the  
460 Swiss National foundation grant BSCGI0\_157800 (SL), a Whitaker International Scholars  
461 Program fellowship to MGP, and an internal pilot grant of the University of Fribourg to MC.

462

#### **Author Contributions**

463 MC, BB and SC conceived the study; BB, MGP, and TM designed and implemented the hardware  
464 and software tools; SC designed the behavioral task and training strategy; GS and SL designed  
465 and manufactured the implantable interface; BB, SC, MGP and MC conducted the experiments;  
466 BB, SC, MGP and KZ performed the data analysis; SC, MD and MK trained the animals; SC, KG,  
467 NJ and QB processed the histological data; JB, GC and MC designed surgical implantation  
468 strategies and stimulation strategies. GC and JB, performed surgical implantations and lesions.  
469 EMR and MC implemented and supervised procedures on monkeys; MC, BB, SC and MGP wrote  
470 the manuscript; all authors edited the manuscript; SL, TM, JB, GC and MC secured funding for  
471 the study; MC supervised the study.

472

475

476 **Competing Interests**

477 G.C., J.B., S.L., M.C., B.B. and K.Z. hold various patents in relation to the present work. G.C.,  
 478 S.L. and J.B. are founders and shareholders of Onwarrd medical, a company developing an EES-  
 479 based therapy to restore movement after spinal cord injury. MC is founder and shareholder of  
 480 Reach Neuro, Inc. a company developing spinal cord stimulation technologies for stroke. All the  
 481 other authors declare no financial interest.

482

483

484 **REFERENCES**

485

1. ICCP. International Campaign for Cures of Spinal Cord Injury Paralysis. <http://www.campaignforcure.org>.
2. National Center for Chronic Disease Prevention and Health Promotion , Division for Heart Disease and Stroke. Stroke Facts. <https://www.cdc.gov/stroke/facts.htm> (2020).
3. Anderson, K. D. Targeting recovery: priorities of the spinal cord-injured population. *Journal of neurotrauma* **21**, 1371–1383 (2004).
4. Moreland, J. D. et al. Needs assessment of individuals with stroke after discharge from hospital stratified by acute Functional Independence Measure score. *Disability and rehabilitation* **31**, 2185–2195 (2009).
5. Lemon, R. N. Descending pathways in motor control. *Annual review of neuroscience* **31**, 195–218 (2008).
6. Griffin, D. M. & Strick, P. L. The motor cortex uses active suppression to sculpt movement. *Sci Adv* **6**, eabb8395 (2020).
7. Seki, K., Perlmutter, S. I. & Fetz, E. E. Sensory input to primate spinal cord is presynaptically inhibited during voluntary movement. *Nat Neurosci* **6**, 1309–16 (2003).
8. Lebedev, M. A. & Nicolelis, M. A. Brain-machine interfaces: From basic science to neuroprostheses and neurorehabilitation. *Physiological reviews* (2017).
9. Nishimura, Y., Perlmutter, S. I. & Fetz, E. E. Restoration of upper limb movement via artificial corticospinal and musculospinal connections in a monkey with spinal cord injury. *Frontiers in neural circuits* **7**, 57 (2013).
10. Shafechi, M. M., Hu, R. C. & Williams, Z. M. A cortical-spinal prosthesis for targeted limb movement in paralysed primate avatars. *Nat Commun* **5**, 3237 (2014).
11. Zimmermann, J. B. & Jackson, A. Closed-loop control of spinal cord stimulation to restore hand function after paralysis. *Front Neurosci* **8**, 87 (2014).
12. Ethier, C., Oby, E. R., Bauman, M. J. & Miller, L. E. Restoration of grasp following paralysis through brain-controlled stimulation of muscles. *Nature* **485**, 368–371 (2012).
13. Bouton, C. E. et al. Restoring cortical control of functional movement in a human with quadriplegia. *Nature* (2016) doi:10.1038/nature17435.
14. Ajiboye, A. B. et al. Restoration of reaching and grasping movements through brain-controlled muscle stimulation in a person with tetraplegia: a proof-of-concept demonstration. *The Lancet* (2017) doi:10.1016/S0140-6736(17)30601-3.

- 520 15. Giat, Y., Mizrahi, J. & Levy, M. A musculotendon model of the fatigue profiles of  
521 paralyzed quadriceps muscle under FES. *IEEE transactions on biomedical*  
522 *engineering* **40**, 664–674 (1993).
- 523 16. Edgerton, V. R. *et al.* Training locomotor networks. *Brain Res Rev* **57**, 241–254  
524 (2008).
- 525 17. Holinski, B. J. *et al.* Intrapinal microstimulation produces over-ground walking in  
526 anesthetized cats. *J Neural Eng* **13**, 056016 (2016).
- 527 18. Capogrosso, M. *et al.* A computational model for epidural electrical stimulation of  
528 spinal sensorimotor circuits. *The Journal of neuroscience : the official journal of the*  
529 *Society for Neuroscience* **33**, 19326–40 (2013).
- 530 19. Formento, E. *et al.* Electrical spinal cord stimulation must preserve proprioception to  
531 enable locomotion in humans with spinal cord injury. *Nature neuroscience* **21**, 1728  
532 (2018).
- 533 20. Wagner, F. B. *et al.* Targeted neurotechnology restores walking in humans with  
534 spinal cord injury. *Nature* **563**, 65 (2018).
- 535 21. Angeli, C. A., Edgerton, V. R., Gerasimenko, Y. P. & Harkema, S. J. Altering spinal  
536 cord excitability enables voluntary movements after chronic complete paralysis in  
537 humans. *Brain* **137**, 1394–1409 (2014).
- 538 22. Ichiyama, R. M., Gerasimenko, Y. P., Zhong, H., Roy, R. R. & Edgerton, V. R.  
539 Hindlimb stepping movements in complete spinal rats induced by epidural spinal  
540 cord stimulation. *Neurosci Lett* **383**, 339–44 (2005).
- 541 23. Courtine, G. *et al.* Transformation of nonfunctional spinal circuits into functional  
542 states after the loss of brain input. *Nat Neurosci* **12**, 1333–1342 (2009).
- 543 24. van den Brand, R. *et al.* Restoring Voluntary Control of Locomotion after Paralyzing  
544 Spinal Cord Injury. *Science* **336**, 1182–1185 (2012).
- 545 25. Grahn, P. J. *et al.* Enabling Task-Specific Volitional Motor Functions via Spinal Cord  
546 Neuromodulation in a Human With Paraplegia. *Mayo Clin Proc* **92**, 544–554 (2017).
- 547 26. Angeli, C. A. *et al.* Recovery of Over-Ground Walking after Chronic Motor Complete  
548 Spinal Cord Injury. *N Engl J Med* **379**, 1244–1250 (2018).
- 549 27. Gill, M. L. *et al.* Neuromodulation of lumbosacral spinal networks enables  
550 independent stepping after complete paraplegia. *Nat Med* (2018)  
551 doi:10.1038/s41591-018-0175-7.
- 552 28. Alam, M. *et al.* Evaluation of optimal electrode configurations for epidural spinal cord  
553 stimulation in cervical spinal cord injured rats. *Journal of neuroscience methods* **247**,  
554 50–57 (2015).
- 555 29. Lu, D. C. *et al.* Engaging Cervical Spinal Cord Networks to Reenable Volitional  
556 Control of Hand Function in Tetraplegic Patients. *Neurorehabil Neural Repair* **30**,  
557 951–962 (2016).
- 558 30. Inanici, F., Brighton, L. N., Samejima, S., Hofstetter, C. P. & Moritz, C. T.  
559 Transcutaneous spinal cord stimulation restores hand and arm function after spinal  
560 cord injury. *IEEE Trans Neural Syst Rehabil Eng* Online ahead of print-Online ahead  
561 of print (2021) doi:10.1109/TNSRE.2021.3049133.
- 562 31. Kapadia, N., Zivanovic, V. & Popovic, M. Restoring voluntary grasping function in  
563 individuals with incomplete chronic spinal cord injury: pilot study. *Topics in spinal*  
564 *cord injury rehabilitation* **19**, 279–287 (2013).

- 565 32. Grillner, S. The motor infrastructure: from ion channels to neuronal networks. *Nat Rev Neurosci* **4**, 573–586 (2003).
- 566 33. Giszter, S. F. Motor primitives--new data and future questions. *Curr Opin Neurobiol* **33**, 156–65 (2015).
- 569 34. Lemon, R. N. & Griffiths, J. Comparing the function of the corticospinal system in  
570 different species: organizational differences for motor specialization? *Muscle &*  
571 *Nerve: Official Journal of the American Association of Electrodiagnostic Medicine* **32**, 261–279 (2005).
- 573 35. Kinoshita, M. et al. Genetic dissection of the circuit for hand dexterity in primates.  
574 *Nature* **487**, 235–238 (2012).
- 575 36. Weiler, J., Gribble, P. L. & Pruszynski, J. A. Spinal stretch reflexes support efficient  
576 hand control. *Nat. Neurosci* 1–11 (2019).
- 577 37. Sauerbrei, B. A. et al. Cortical pattern generation during dexterous movement is  
578 input-driven. *Nature* **577**, 386–391 (2020).
- 579 38. Capogrosso, M. et al. Configuration of electrical spinal cord stimulation through real-  
580 time processing of gait kinematics. *Nat Protoc* (2018) doi:10.1038/s41596-018-  
581 0030-9.
- 582 39. Capogrosso, M. et al. A brain-spine interface alleviating gait deficits after spinal cord  
583 injury in primates. *Nature* **539**, 284–288 (2016).
- 584 40. Greiner, N. et al. Recruitment of Upper-Limb Motoneurons with Epidural Electrical  
585 Stimulation of the Primate Cervical Spinal Cord. *Nat Commun* (2021).
- 586 41. Barra, B. et al. A Versatile Robotic Platform for the Design of Natural, Three-  
587 Dimensional Reaching and Grasping Tasks in Monkeys. *Journal of Neural*  
588 *Engineering* (2019) doi:10.1088/1741-2552/ab4c77.
- 589 42. Capogrosso, M. et al. A brain-spine interface alleviating gait deficits after spinal cord  
590 injury in primates. *Nature* **539**, 284–288 (2016).
- 591 43. Schiavone, G. et al. Soft, Implantable Bioelectronic Interfaces for Translational  
592 Research. *Advanced Materials* **32**, 1906512 (2020).
- 593 44. Chao, Z. C., Sawada, M., Isa, T. & Nishimura, Y. Dynamic Reorganization of Motor  
594 Networks During Recovery from Partial Spinal Cord Injury in Monkeys. *Cereb Cortex*  
595 (2018) doi:10.1093/cercor/bhy172.
- 596 45. Freund, P. et al. Nogo-A-specific antibody treatment enhances sprouting and  
597 functional recovery after cervical lesion in adult primates. *Nature medicine* **12**, 790–  
598 792 (2006).
- 599 46. Sharpe, A. N. & Jackson, A. Upper-limb muscle responses to epidural, subdural and  
600 intraspinal stimulation of the cervical spinal cord. *J Neural Eng* **11**, 016005 (2014).
- 601 47. Gallego, J. A., Perich, M. G., Miller, L. E. & Solla, S. A. Neural Manifolds for the  
602 Control of Movement. *Neuron* **94**, 978–984 (2017).
- 603 48. Kato, K., Nishihara, Y. & Nishimura, Y. Stimulus outputs induced by subdural  
604 electrodes on the cervical spinal cord in monkeys. *Journal of Neural Engineering* **17**,  
605 016044 (2020).
- 606 49. de Freitas, R. M. et al. Selectivity and excitability of upper-limb muscle activation  
607 during cervical transcutaneous spinal cord stimulation in humans. *Journal of Applied*  
608 *Physiology* (2021).

- 609 50. Kirsch, R. & Rymer, W. Neural compensation for muscular fatigue: evidence for  
610 significant force regulation in man. *Journal of neurophysiology* **57**, 1893–1910  
611 (1987).
- 612 51. Song, S. & Geyer, H. A neural circuitry that emphasizes spinal feedback generates  
613 diverse behaviours of human locomotion. *The Journal of physiology* (2015)  
614 doi:10.1113/JP270228.
- 615 52. Seáñez, I. & Capogrosso, M. Motor improvements enabled by spinal cord  
616 stimulation combined with physical training after spinal cord injury: review of  
617 experimental evidence in animals and humans. *Bioelectronic Medicine* **7**, 1–13  
618 (2021).
- 619 53. Granat, M., Heller, B., Nicol, D., Baxendale, R. & Andrews, B. Improving limb flexion  
620 in FES gait using the flexion withdrawal response for the spinal cord injured person.  
621 *Journal of biomedical engineering* **15**, 51–56 (1993).
- 622 .  
623  
624

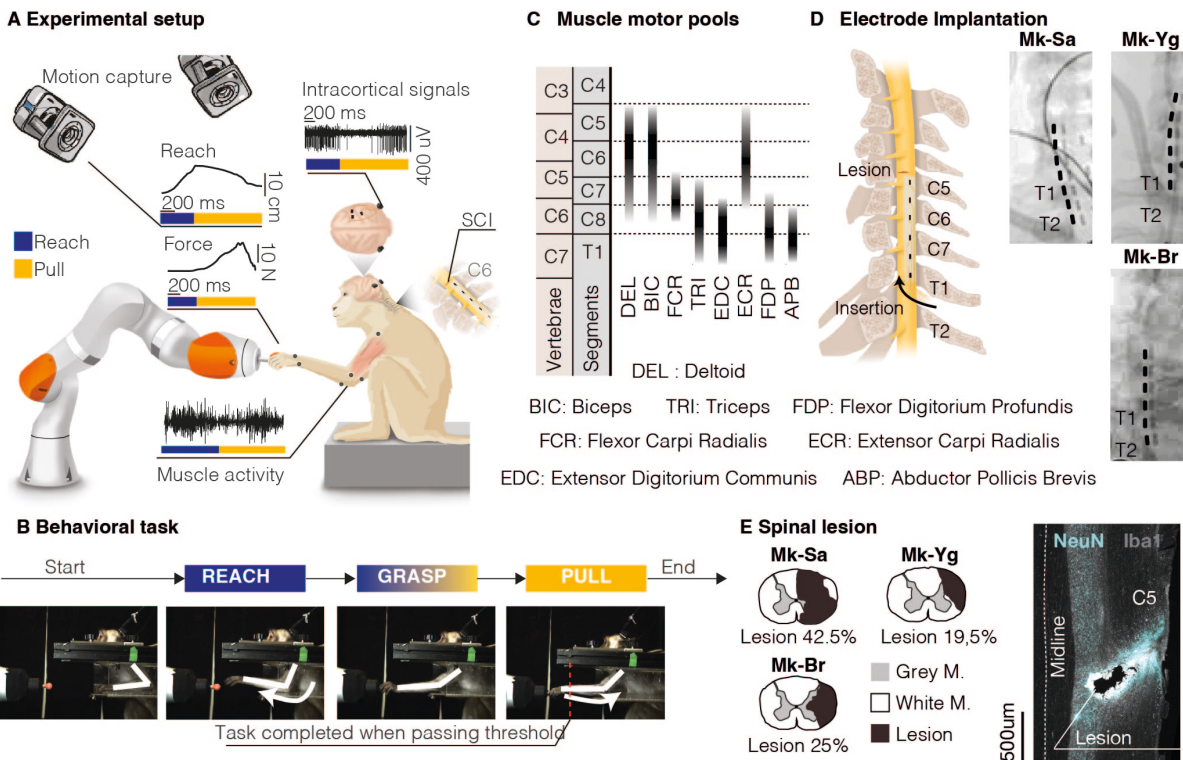


**Figure 1. Experimental framework.** **(A)** Schematic of the behavioral experimental platform. While the animals were performing a robotic reach, grasp and pull task, we measured 3D forces applied to the robot joints, full-limb kinematics, electromyographic (EMG) activity from eight muscles of the arm and hand, and intra-cortical signals from sensorimotor areas. **(B)** Schematic illustration of the task. Monkeys were trained to reach for, grasp, and pull a target object placed at the end effector of a robotic arm. We considered a movement complete when a target spatial threshold was crossed during pull. **(C)** Motoneurons pool distribution of arm and hand muscles in the cervical spinal cord in relation to vertebrae and spinal segments (adapted from Jenny and Inukai, 1983). Deltoid (DEL), Biceps Brachii (BIC), Flexor Carpi Radialis (FCR), Triceps Brachii (TRI), Extensor Digitorum Communis (EDC), Extensor Carpi Radialis (ECR), Flexor Digitorum Profundis (FDP), Abductor Pollicis Brevis (ABP). **(D)** Schematic representation of spinal implant positioning and X-ray scans of the epidural implant in the three monkeys (Mk-Sa, Mk-Br and Mk-Yg). **(E)** Anatomical reconstruction of the cervical spinal cord lesion (black area) for the 3 monkeys, shown on a transversal section (the percentage indicates the portion of the total spinal cord area that was injured on this transversal plane). On the right, representative image of longitudinal section of the spinal cord of Mk-Br around the lesion site stained with NeuN (neuronal cell bodies) and Iba1 (microglia). Copyright Jemère Ruby.

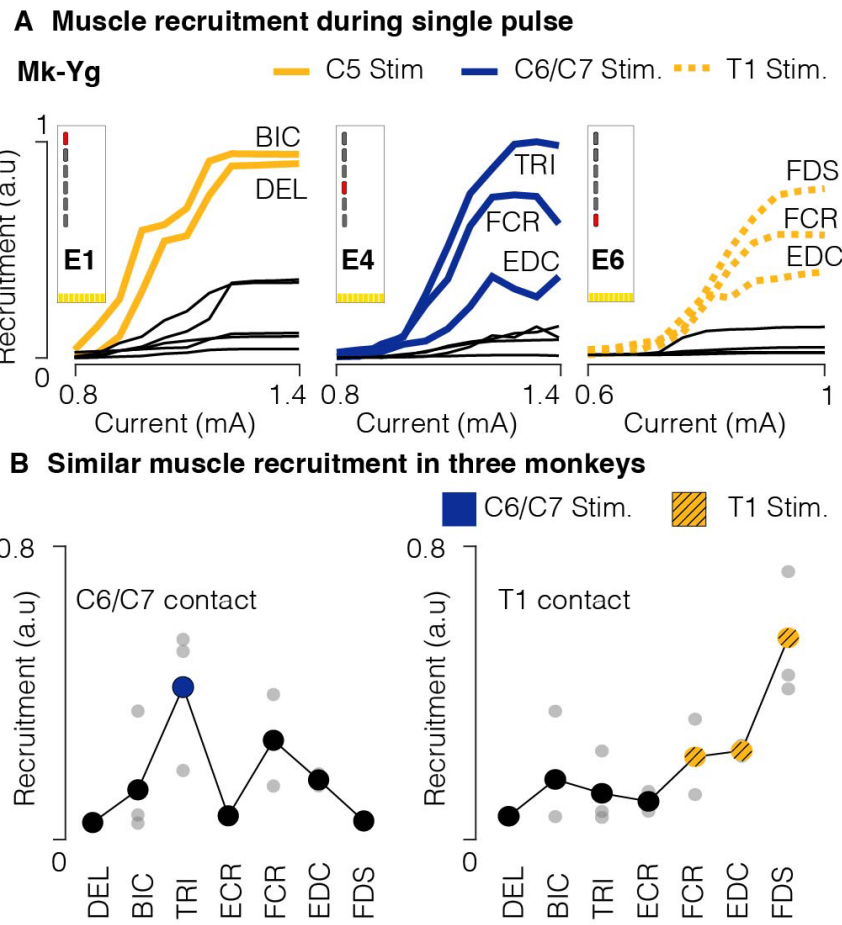


**Figure 2. Muscle recruitment of spinal stimulation. (A)** Examples of muscle recruitment obtained by stimulating (1 Hz) at C5, C6/C7, and T1 spinal segments (Mk-Yg). **(B)** Average muscle activations elicited from C6/C7 and T1 contacts in n=3 monkeys (grey bullets: for each animal, average recruitment across all stimulation currents. Big bullets: mean of average recruitments across animals).

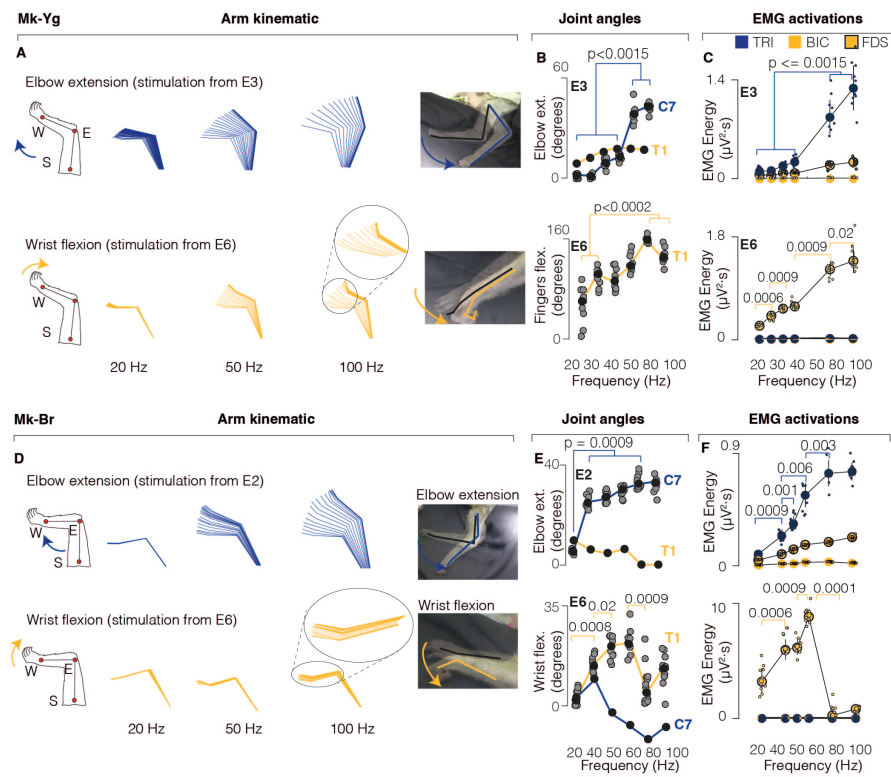
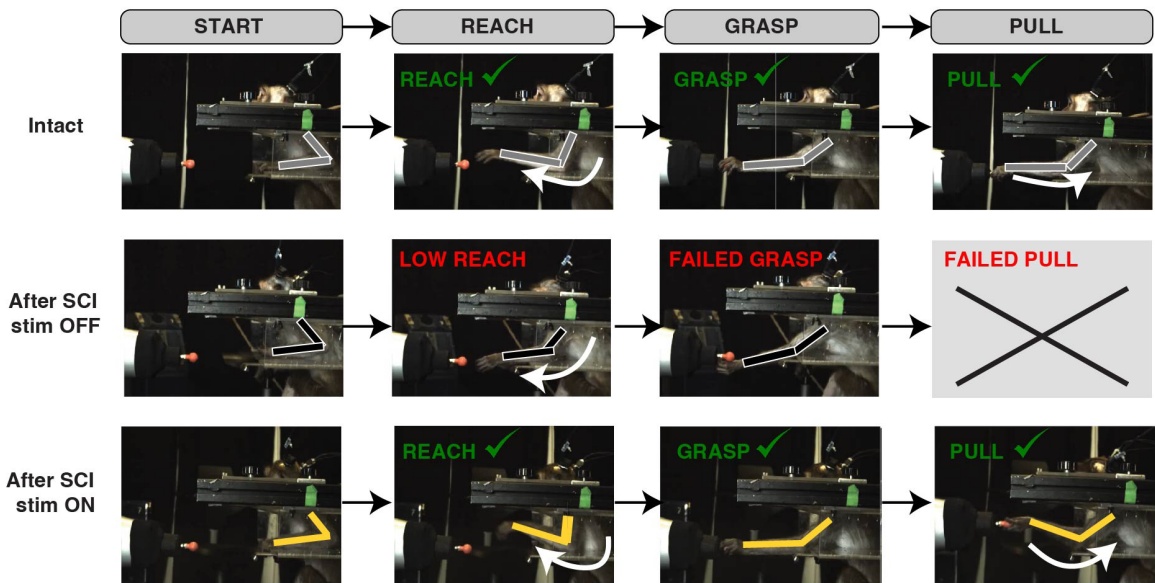


**Figure 3. EES produces functional joint movements in anesthetized animals.** (A) Stick diagram schematic of elbow extension and wrist flexion movements elicited by pulse-trains of stimulation in anesthetized conditions in Mk-Yg from the electrode contacts 3 and 6 (E3 and E6). (B) Modulation of maximal joint angles achieved by pulse-trains of stimulation at different frequencies, in anesthetized conditions in Mk-Yg. Stimulation was delivered at C7 (blue, n = 12, 10, 11, 10, 10, 10 independent samples) and T1 (yellow, n = 11, 10, 10, 10, 10, 13 independent samples). Black bullets represent median values, gray bullets are individual datapoints. Statistics performed with two-sided Wilcoxon Ranksum test and Bonferroni correction. (C) Triceps (blue), biceps (yellow), and flexor digitorium superficialis (yellow with black border) activity elicited by pulse-trains of stimulation at different frequencies, in anesthetized conditions in Mk-Yg. Top, activation during stimulation from electrode contact E3 (from left to right, n = 12, 10, 11, 10, 10, 10 independent samples). Bottom, activation during stimulation from electrode contact E6 (from left to right, n = 11, 10, 10, 10, 10, 13 independent samples). Bullets represent median values and bars are standard deviation. Statistics performed with two-sided Wilcoxon Ranksum test and Bonferroni correction. (D) Stick diagram schematic of elbow extension and wrist flexion movements elicited by pulse-trains of stimulation in anesthetized conditions in Mk-Br from the electrode contacts 2 and 6 (E2 and E6). (E) Modulation of maximal joint angles achieved by pulse-trains of stimulation at different frequencies, in anesthetized conditions in Mk-Br. Stimulation was delivered at C7 (blue, n = 10, 10, 10, 10, 10 independent samples) and T1 (yellow, n = 10, 11, 10, 10, 15, 11 independent samples). Statistics performed with two-sided Wilcoxon Ranksum test and Bonferroni correction. Black bullets represent median values, gray bullets are individual datapoints. (F) Triceps (blue), biceps (yellow), and flexor digitorium superficialis (yellow with black border) activity elicited by pulse-trains of stimulation at different frequencies, in anesthetized conditions in Mk-Br. Top, activation during stimulation from electrode contact E2 (from left to right, n = 10, 10, 10, 10, 10 independent samples). Bottom, activation during stimulation from electrode contact E6 (from left to right, n = 10, 11, 10, 10, 15, 11 independent samples). Bullets represent median values and bars are standard deviation. Statistics performed with two-sided Wilcoxon Ranksum test and Bonferroni correction.

## A Example of task performance, Mk-Yg



B

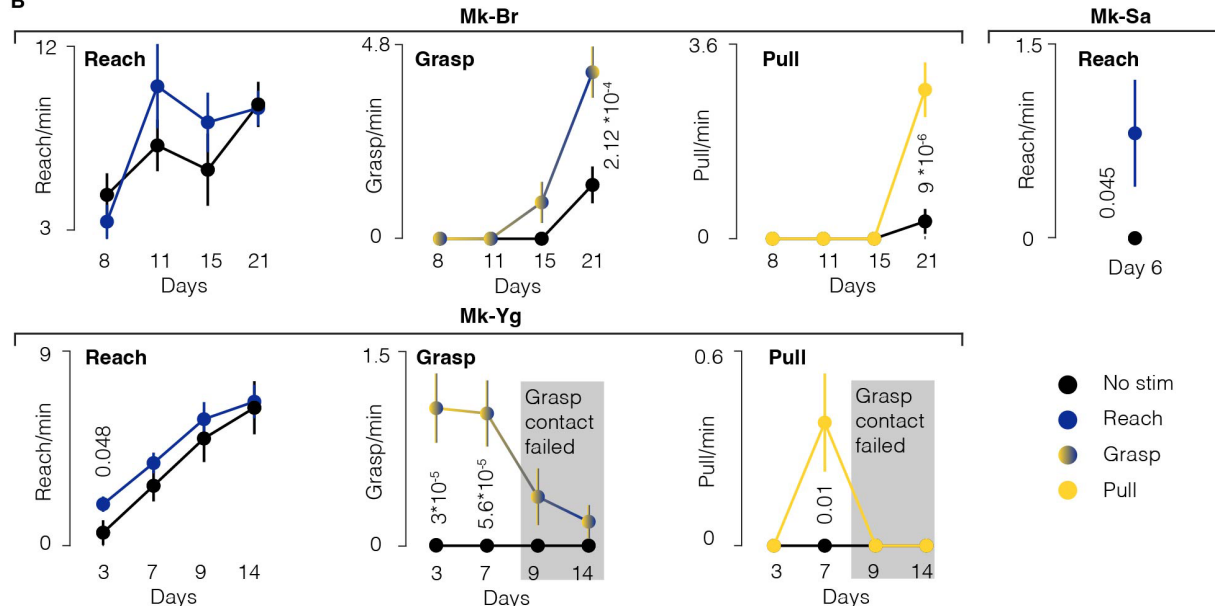


**Figure 4. EES improves task performance.** (A) Snapshots of Mk-Yg performing the task before SCI, after SCI without EES, and after SCI with EES. A full successful trial is composed of a reach, a grasp, and a pull. After SCI, Mk-Yg could only perform reaching movements without EES, while when EES was delivered the full task could be performed. (B) Task rate performance rate over different sessions, computed as the number of successful movements per minute. Performance rate are shown for reach (blue), grasp (yellow to blue gradient) and pull (yellow movements). Data are shown as mean (bullets) and standard deviation (bars). Statistics and significance evaluated by estimating two side residuals via Bootstrap. Asterisks: \*p<0.05, \*\*p<0.01, \*\*\*p<0.001.

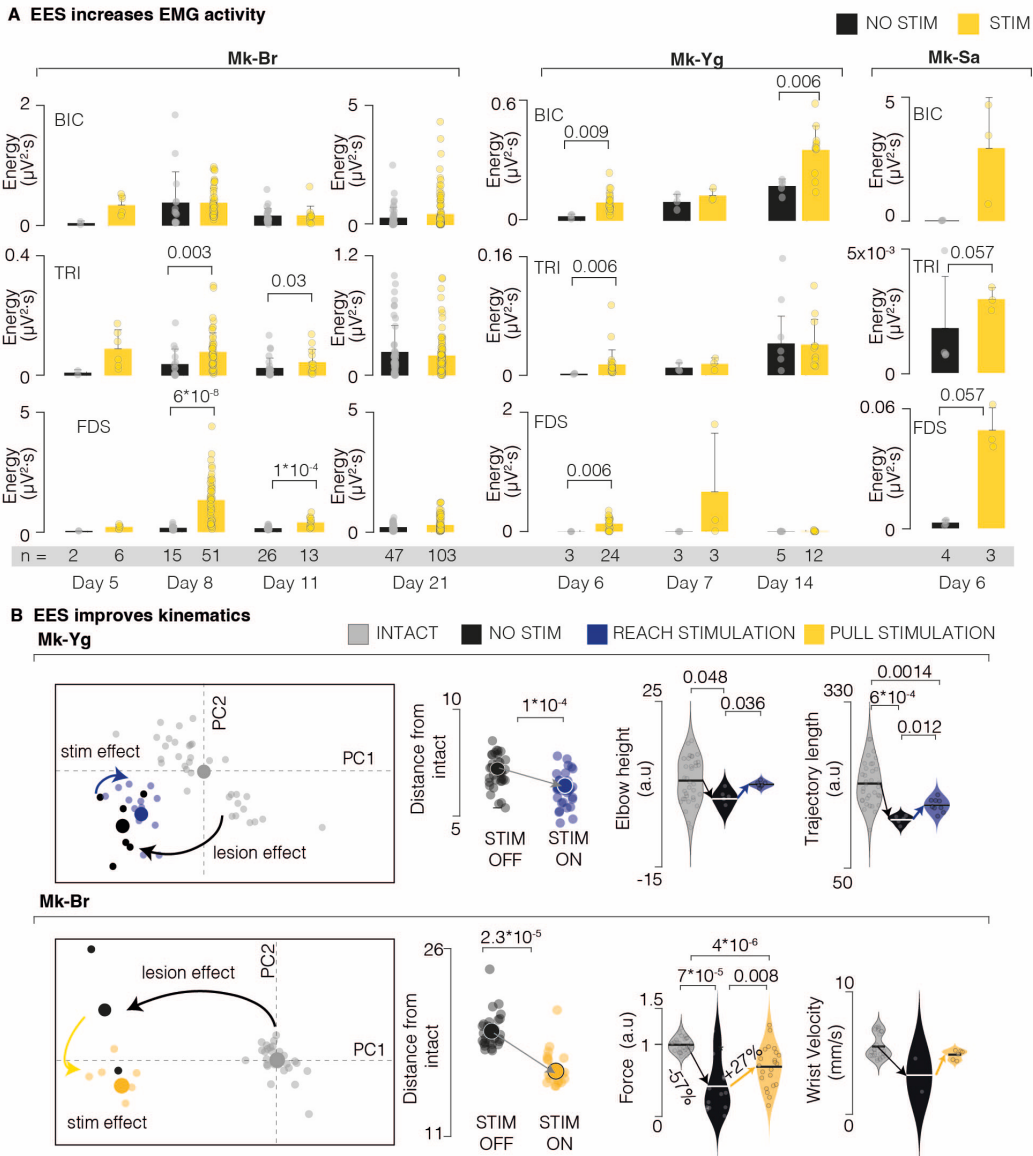


**Figure 5. EES improves muscle strength and movement quality.** (A) Bar plots of signal energy of biceps, triceps and FDS EMG profiles during movement with no stimulation (black) and stimulation (yellow). Data are shown for different sessions (one for each week) in Mk-Br and Mk-Yg. Mk-Sa performed only one session. Data are shown as mean  $\pm$  STD. All individual data points are represented by bullets. Statistical analysis with two-sided Wilcoxon Ranksum test. (B) Kinematic features for Mk-Yg (top) and Mk-Br (bottom) are displayed in a new space created by principal component 1 (PC1) and principal component 2 (PC2). From left to right: (1) first and second PC space. Each bullet represents one trial. Trials performed after injury (black) are consistently separated from the trials performed in intact conditions, highlighting a change in the quality of resulting kinematics. Trials performed with the support of stimulation (blue for reach and yellow for pull) are located closer to the intact trials in the PC space, denoting an improvement in kinematic features. (2) Euclidean distance in the feature space of trials without stimulation (black) and with stimulation (blue for Mk-Yg, yellow for Mk-Br) from the centroid of the trials in intact condition. Statistical analysis with two-sided Wilcoxon Ranksum test. (3) example violin plots of movement quality features in the three conditions: intact, after SCI with stimulation. Statistical analysis with two-sided Wilcoxon Ranksum test.

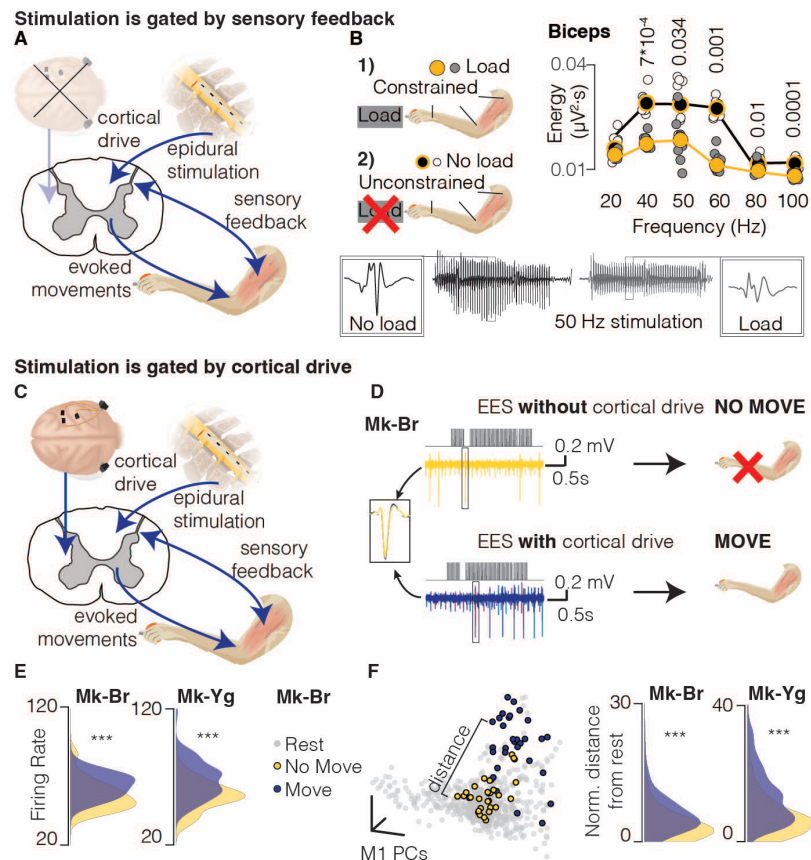
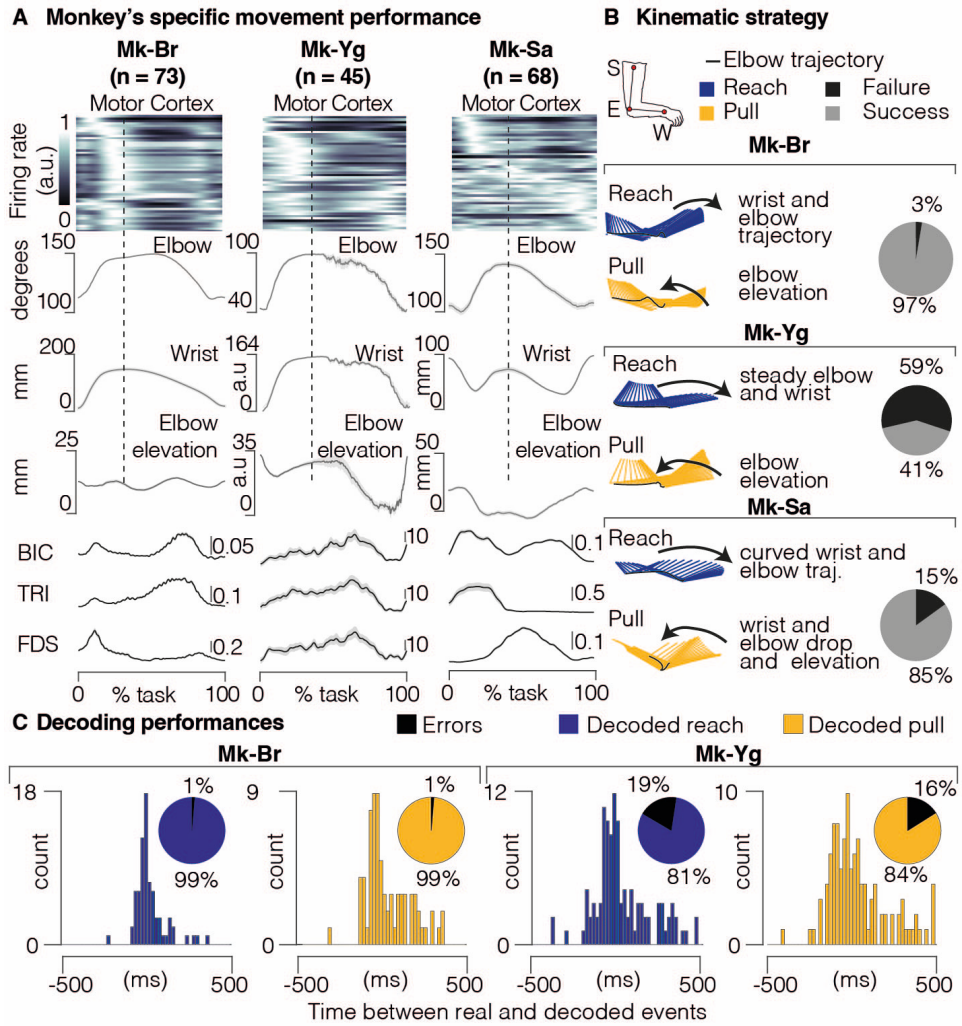
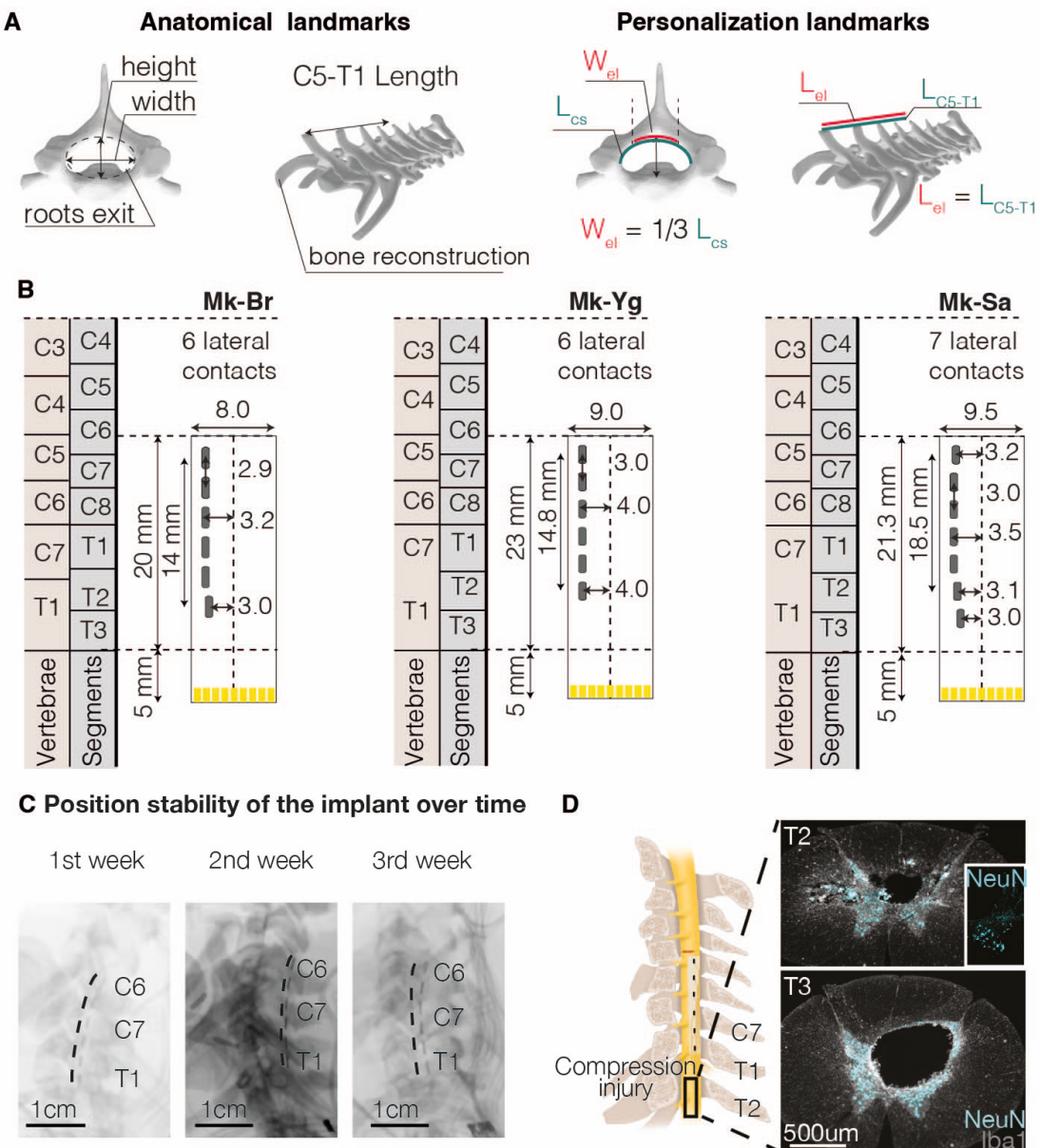


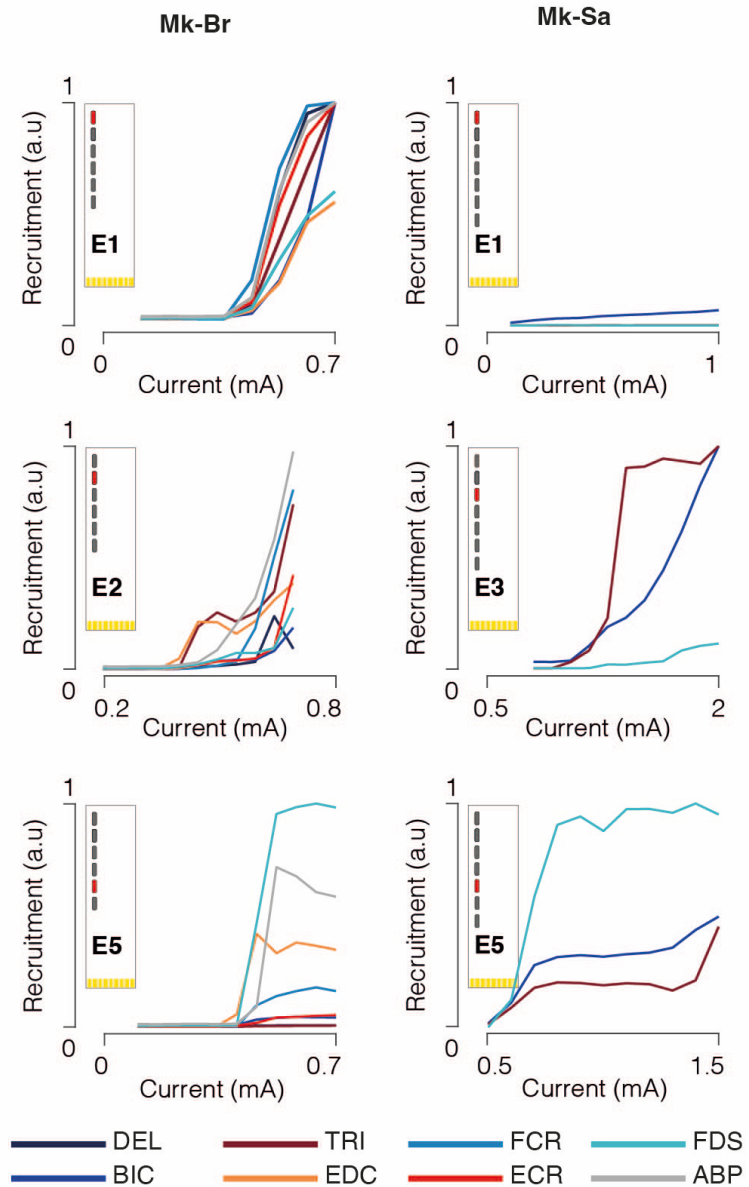
**Figure 6. EES must be synchronized with motor intention.** (A) interactions between EES and residual neural structures during anesthesia. During anesthesia, cortical inputs are absent, therefore EES interacts solely with spinal sensory feedback. (B) Quantification of EMG activity: unconstrained arm (no load, black); arm constrained by load applied at the hand (load, gray). White and grey bullets: individual data points for no load and load conditions. Black and yellow bullets: median values for no load and load conditions. Black and yellow lines: interpolation of median values for no load and load conditions. On the bottom, example of EMG traces obtained during stimulation in the no-load (black) and load (gray) conditions. Stimulation artifacts have been removed. Data from Mk-Br (C) Interactions between EES and residual neural structures in awake monkeys. EES interacts with residual descending cortical drive after SCI and with spinal sensory inputs. (D) Schematic illustrating the kinematic outcome of the interaction between EES and residual cortical inputs. The same EES pulse train (top) applied to Mk-Br can result in different motor outputs: no movement output when the cortex is silent (yellow, top), movement is produced when the cortex is active (blue, bottom). (E) Distribution of average firing rates across all M1 channels during stimulation trains that evoked no movement (yellow) and movement (blue). Statistical analysis with two-sided Wilcoxon Ranksum test (Mk-Br,  $p = 1.19e^{-18}$ ; Mk-Yg,  $p = 2.82e^{-118}$ ) (F) Left: State space view of M1 activity for all time points during rest (gray), successful stimulation (blue) and unsuccessful stimulation (yellow). The brain states during unsuccessful stimulation (yellow) overlapped with the rest states, while the successful stimulation (blue) did not. Right: we computed a relative Mahalanobis distance between the two stimulation conditions and the cluster of neural states at rest. For both monkeys, neural states during stimulation periods with no movement were close to rest. Statistical analysis with two-sided Wilcoxon Ranksum test (Mk-Br,  $p = 5.69e^{-96}$ ; Mk-Yg,  $p = 5.36e^{-11}$ ).



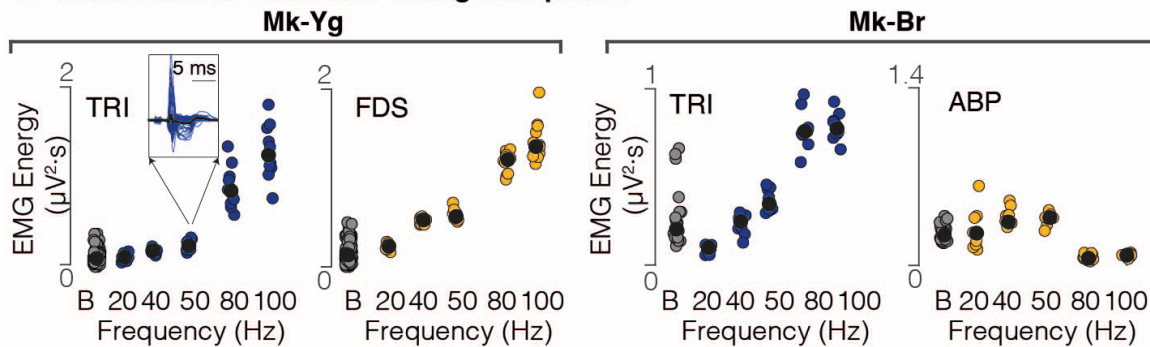
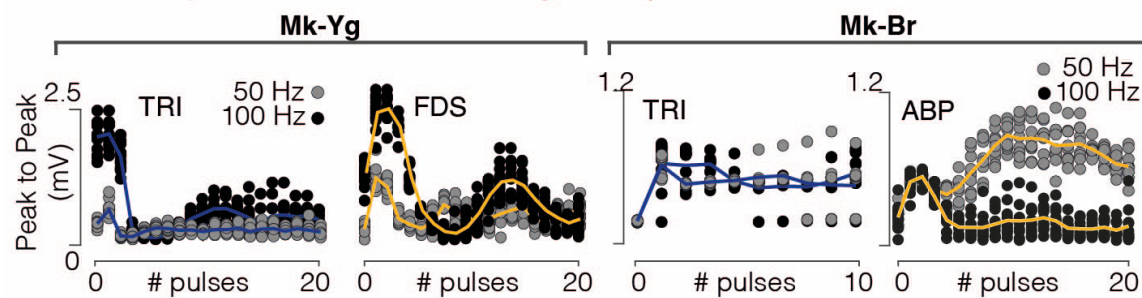
**Extended Data Figure 1.** **(A)** Portfolio of signals recorded during intact movement for each animal. These signals have been recorded during the experimental session prior to the lesion. Motor cortex recordings show firing rate profiles for the 64 microelectrodes. Each row shows the firing rate of a specific electrode. Electrodes are displayed from top to bottom by order of first activation in a reference trial. Arbitrary units in motor cortex recording indicate normalized firing rate for each electrode (see methods). In kinematic and EMG plots, black lines correspond to the mean profile across all trials, shaded area shows the SEM across all trials. Kinematic scales are expressed in mm. For Mk-Yg, arbitrary units on kinematic plots represent displacement units derived by the count of video pixels. EMG scales are expressed in mV. **(B)** Kinematic strategies implemented by each monkey. Stick diagrams representations of the arm kinematic during reach (blue) and pull (yellow). The black line highlights the elbow trajectory. Pie charts represent the percentage of success and failure in task performance before lesion. **(C)** Offline decoding performance for Mk-Br and Mk-Yg before lesion. Histograms show timing accuracy of reach (blue) and pull (yellow) event decoding. The height of bars (y coordinate) illustrates the amount of events decoded with a specific timing accuracy (x coordinate). Pie charts (inset) show the percentage of correctly identified (true positive) reaches (blue) and pulls (yellow), across all decoded events. The black portion of the pie chart highlights the percentage of false positive decoded events.



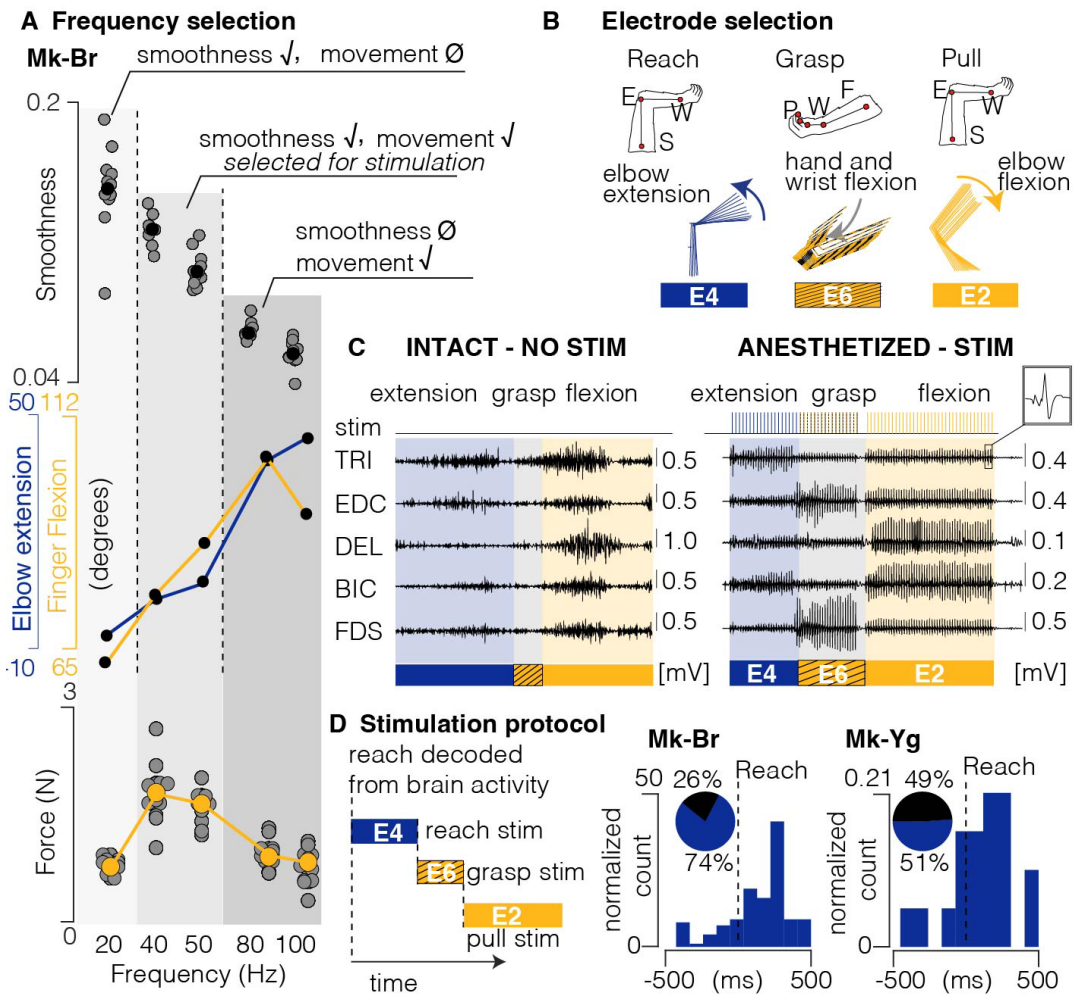
**Extended Data Figure 2.** **(A)** Anatomical landmarks used to tailor the epidural interface to each monkey's anatomy (Length of dorsal aspect of spinal canal  $L_{cs}$ , length of C5-T1 spinal segment  $L_{C5-T1}$ , electrode width  $W_{el}$ , electrode length  $L_{el}$ ). Three-dimensional reconstructions of vertebrae are obtained by CT-reconstruction (Osirix, Pixmeo, Switzerland). **(B)** Personalized design of the epidural implant for each animal. All measures are in millimeters. Yellow traces at the bottom of the electrode identify connectors. **(C)** Position stability of the epidural array over time, illustrated through X-rays imaging taken during 3 consecutive weeks after the implantation, images from Mk-Yg **(D)** Compression injury at the insertion level of the array (T2-T3 segment) in Mk-Br, discovered post-mortem, stained with NeuN (neuronal cell bodies) and Iba1 (microglia).

**Recruitment curves**

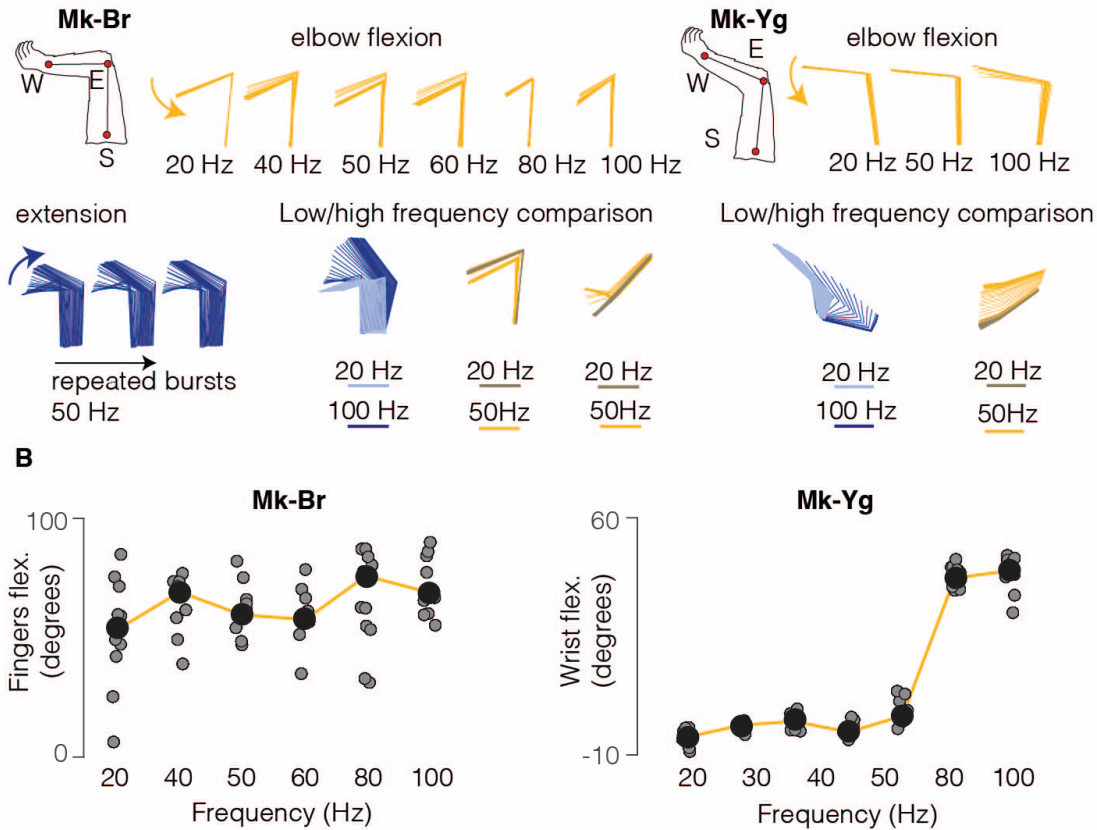
**Extended Data Figure 3.** Muscle recruitment obtained by stimulating, through different electrode contacts (E1, E2, E3, E5), at 1 Hz at C5, C6/C7, and T1 spinal segments for Mk-Br and Mk-Sa. Mk-Sa only had three muscles implanted: biceps, triceps, and flexor digitorium superficialis.

**A Graded muscle activation during train pulses****B Muscle responses are modulated at higher frequencies**

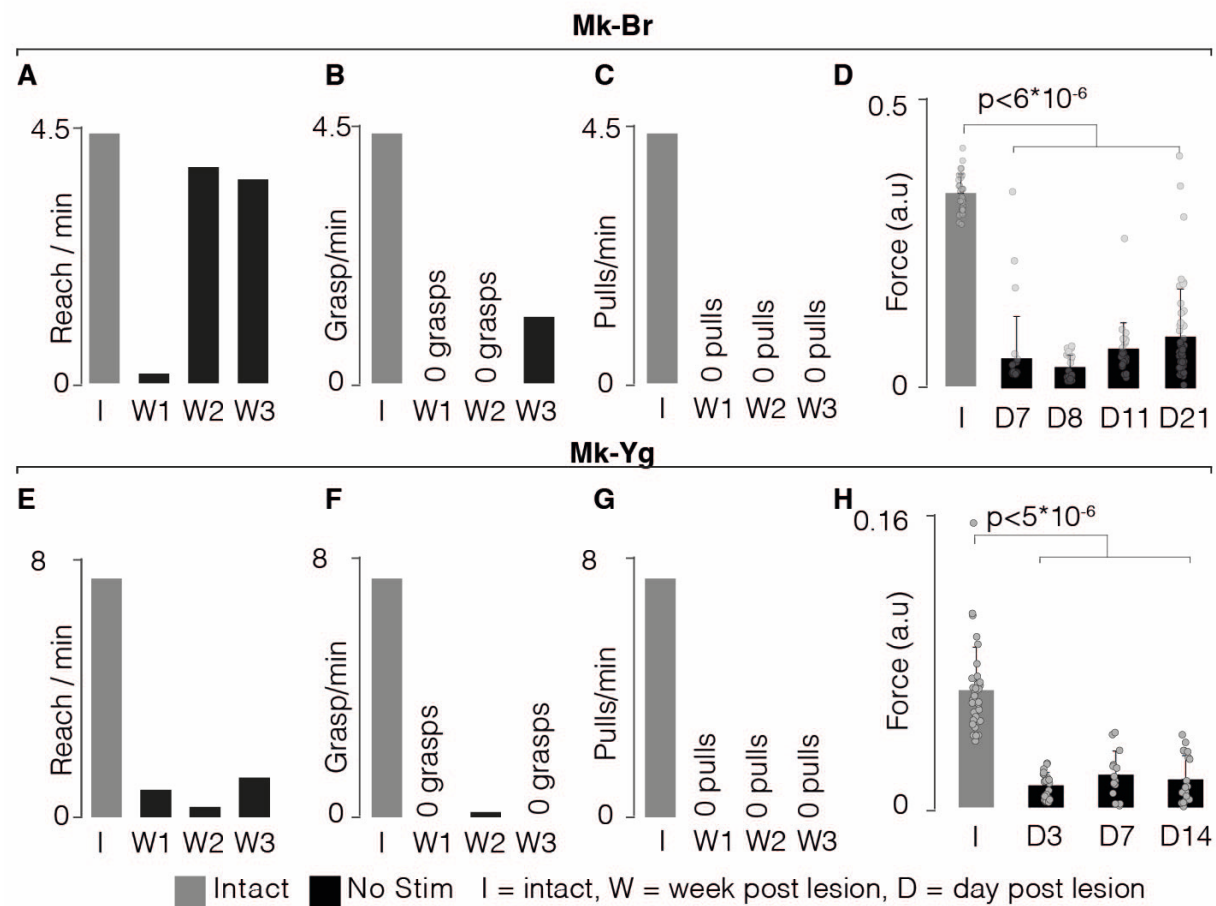
**Extended Data Figure 4. (A)** Energy of EMG signals of triceps (Mk-Br and Mk-Yg), Flexor Digitorium Superficialis (Mk-Yg) and abductor pollicis (Mk-Br) muscles, following pulse-train stimulation at different frequencies (on the x-axis). Black bullets represent mean values. **(B)** Evolution over time of the peak-to-peak value of stimulation evoked responses during a stimulation burst. Each plot shows the evolution for a specific muscle following pulse-train stimulation at 50 and 100Hz. Triceps is shown for Mk-Br and Mk-Yg, Flexor Digitorium Superficialis for Mk-Yg and abductor pollicis for Mk-Br. Each data point is represented as a bullet and lines represent mean values over time.



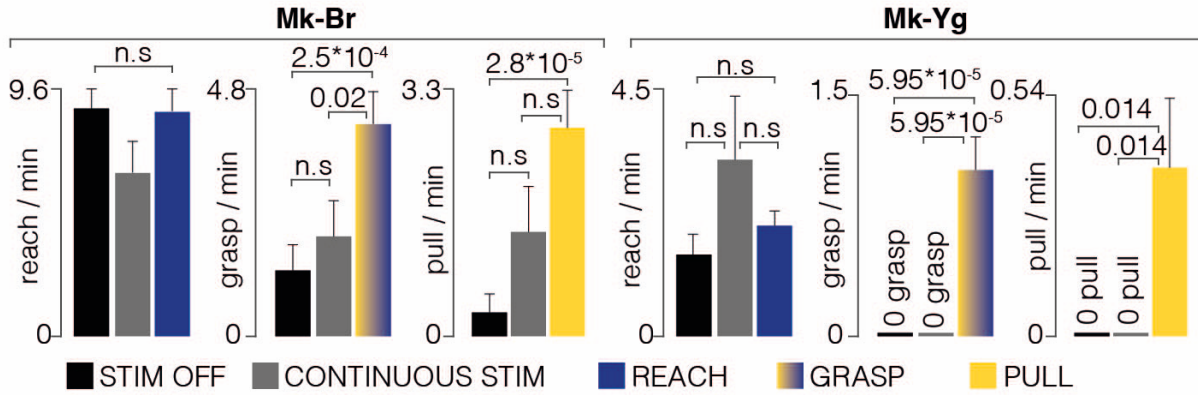
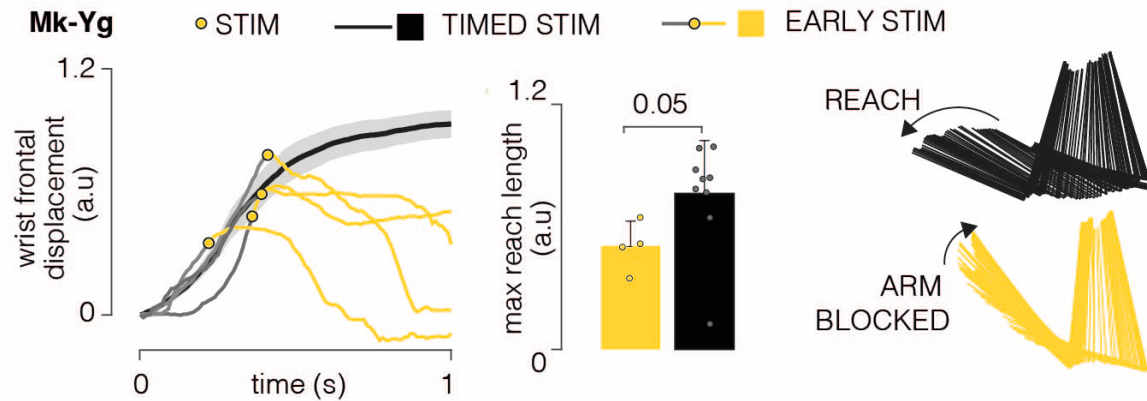
**Extended Data Figure 5.** **(A)** Combined representation of movement smoothness, elbow and finger flexion, and pulling force during anesthetized stimulation. Shades of gray highlight three frequency ranges that produce: (1) smooth trajectory, but little movement and low force (20Hz), (2) smooth trajectory, extended movement and medium force (40 and 50Hz), (3) abrupt and very extended movement and low force (80 and 100Hz). Kinematics and force reported here were measured in different experiments, kinematics was unconstrained, force data were acquired in isometric conditions (see Methods). The range 40-50 Hz was selected as the best optimization of sufficient movement, smoothness and force production. **(B)** Schematic representation of arm and hand kinematics during stimulation delivered from the selection of three contacts to produce elbow extension (blue), hand and wrist flexion (yellow and black), and elbow flexion (yellow). **(C)** Example of comparison between EMG activity during intact movement (left) and movement elicited by chaining stimulation from the three selected contacts (right). **(D)** Scheme illustrating how stimulation is triggered from movement-related intra-cortical signals. On the right, online performances of movement attempt decoder in two animals with SCI. Pie charts represent percentage of predicted (blue) and unpredicted (black) reach events by our decoder.

**A Arm movement is modulated by stimulation frequency**


**Extended Data Figure 6.** **(A)** Stick diagram schematic of movements elicited by pulse-trains of stimulation in anesthetized conditions. Mk-Br: on the left, arm kinematic obtained by delivering stimulation at different frequencies from contact number 5, on the bottom-left, arm kinematics obtained by repetitive delivery of a burst at 50 Hz; on the bottom right, superimposition of stick diagrams obtained with stimulation at 20 Hz and at higher frequencies (50 or 100 Hz) from different contacts. For Mk-Yg: arm kinematic obtained by delivering stimulation at different frequencies from contact number 2 and superimposition of stick diagrams obtained with stimulation at 20 Hz and at higher frequencies (50 or 100 Hz) from different contacts. **(B)** On the left, finger flexion produced by stimulation at different frequencies from the grasp contact in Mk-Br. Black bullets represent the mean value across different pulse-trains. On the right, wrist flexion obtained by stimulation at different frequencies from the grasp contact in Mk-Yg.



**Extended Data Figure 7.** **(A)** Evolution (in weeks) of rates at which Mk-Br performed reach movements after SCI (black), compared to the performances before injury (gray). **(B)** Evolution (in weeks) of rates at which Mk-Br performed grasp movements after SCI (black), compared to the performances before injury (gray). **(C)** Evolution (in weeks) of rates at which Mk-Br performed pull movements after SCI (black), compared to the performances before injury (gray). **(D)** Evolution (in days) of pull force after SCI without stimulation for Mk-Br. Values are plotted as the mean  $\pm$  STD (from left to right, n = 28, 29, 22, 26, 51 independent samples). Statistical analysis was carried out with two-sided Wilcoxon Ranksum test and Tuckey-Cramer correction. **(E)** Evolution (in weeks) of rates at which Mk-Yg performed reach movements after SCI (black), compared to the performances before injury (gray). **(F)** Evolution (in weeks) of rates at which Mk-Yg performed grasp movements after SCI (black), compared to the performances before injury (gray). **(G)** Evolution (in weeks) of rates at which Mk-Yg performed pull movements after SCI (black), compared to the performances before injury (gray). **(H)** Evolution (in days) of pull force after SCI without stimulation for Mk-Yg. Values are plotted as the mean  $\pm$  STD. (from left to right, n = 35, 23, 14, 20, independent samples). Statistical analysis was carried out with two-sided Wilcoxon Ranksum test and Tuckey-Cramer correction.

**A Continuous EES****B Effect of stimulation timing**

**Extended Data Figure 8. (A)** Bar plots report the rate of successful movements after SCI, without stimulation (black), with continuous stimulation (gray) and with phase-dependent stimulation (blue or yellow) for Mk-Br and Mk-Yg. Data are presented as mean  $\pm$  STD and normalized on the mean value in stimulation condition. Significance evaluated by estimating two side residuals via Bootstrap. **(B)** Left: wrist frontal displacement in trials in which pull stimulation was erroneously triggered during reach (gray and yellow), compared to trials in which pull stimulation was not delivered (black, solid line represents the mean and shaded area represents the SEM). Yellow bullets highlight the instant at which stimulation was delivered: yellow lines highlight the trajectories during and after stimulation. Middle: barplot of the length of the reach movement when pull stimulation was erroneously delivered ( $n = 4$ ) and when pull stimulation was not delivered ( $n = 9$ ). Data are presented as mean  $\pm$  STD. Statistics performed with two-sided Wilcoxon Ranksum test. Right: stick diagram of arm kinematics during reach without (black) and with (yellow) erroneous pull stimulation.

645 **METHODS**

646

647 Animals involved in the study

648

649 All procedures were carried out in accordance to the Guide for Care and Use of Laboratory  
650 Animals and the principle of the 3Rs. Protocols were approved by local veterinary authorities of  
651 the Canton of Fribourg (veterinary authorization No 2017\_04\_FR and 2017\_04E\_FR), including  
652 the ethical assessment by the local (cantonal) Survey Committee on Animal Experimentation and  
653 final acceptance by the Federal Veterinary Office (BVET, Bern, Switzerland). Three adult female  
654 *Macaca Fascicularis* monkeys were involved in the study (Mk-Sa 9 years old, 4.0 kg, Mk-Br 3  
655 years old, 3.4 kg, Mk-Yg 3 years old, 4.0 kg). Animals were not food deprived, could freely access  
656 water at any time and were housed in collective rooms designed in accordance to the Swiss  
657 guidelines (detention in groups of 2-5 animals in a room of at least 45 m<sup>3</sup>). Rooms were enriched  
658 with toys, food puzzles, tree branches and devices to climb and hide, as well as access to an  
659 outdoor space of 10-12 m<sup>3</sup> (see [www.unifr.ch/spccr/about/housing](http://www.unifr.ch/spccr/about/housing)). Detailed information on which  
660 animals were involved in specific experimental procedures are reported in **Supplementary Table  
661 1.**

662 Surgical procedures

663 For each animal, we performed three surgical procedures, (1) intracortical electrodes implantation,  
664 (2) intramuscular electrodes implantation, and (3) epidural implant insertion and spinal cord injury.  
665 Mk-Sa deviated from this protocol. Mk-Sa was first implanted with the epidural interface before  
666 injury, however an infection occurred and resulted in the explantation of the lead to treat the  
667 infection. After recovery, the animal was re-implanted, and lesion performed following the same  
668 protocol of Mk-Br and Mk-Yg. All the surgical procedures were performed under full anesthesia  
669 induced with midazolam (0.1 mg/kg, i.m.), methadone (0.2 mg/kg, i.m.), and ketamine (10 mg/kg,  
670 i.m.) and maintained under continuous intravenous infusion of propofol (5 ml/kg/h) and fentanyl  
671 (0.2-1.7 ml/kg/h) using standard aseptic techniques. A certified neurosurgeon (Dr. Jocelyne Bloch,  
672 CHUV, Lausanne, Switzerland) performed all the surgical procedures. A detailed description of  
673 each surgical procedure is reported in the Supplementary information.

674 Data acquisition

675 For Mk-Sa and Mk-Br, we acquired three-dimensional spatial coordinates of arm and hand joints  
676 using a 14-camera motion tracking system (Figure 1, Vicon Motion Systems, Oxford, UK) that  
677 tracked the Cartesian position of 6 infrared reflective markers (6 to 9 mm in diameter each, Vicon  
678 Motion Systems, Oxford, UK) at a 100 Hz framerate. All markers were placed on the left arm, one  
679 below the shoulder, three on the elbow (proximal, medial and distal position), and two on the left  
680 and right side of the wrist. For each subject, a model of the marker placement was calibrated in  
681 Vicon's Nexus software at the beginning of each experimental session. For Mk-Yg spatial  
682 coordinates of arm and hand joints were recorded using two cameras placed parallel to the sagittal  
683 and transversal plane of the animal (Vicon Motion Systems, Oxford, UK). The 3D coordinates of  
684 the arm and hand joints were extracted using DeepLabCut<sup>55</sup>. Due to the reduced informative  
685 content extracted from the camera parallel to the transverse plane, we then only used 2D  
686 coordinates on the animals' sagittal plane. The training set needed for automatic data labeling  
687 was created by manually labeling a subset of recorded videos. An investigator was blinded to the  
688 experimental condition and was instructed to mark four anatomical landmarks that mirrored the  
689 position of markers in Mk-Sa and Mk-Br (shoulder, medial elbow, left and right wrist). Neural

690 signals were acquired with a Neural Signal Processor (Blackrock Microsystems, USA) using the  
691 Cereplex-E headstage with a sampling frequency of 30 kHz. Electromyographic signals were  
692 acquired with a Behavioral Neurophysiology chronic recording system (RZ2 BioAmp Processor,  
693 Tucker-Davis Technologies, USA) at a sampling frequency of 12207 Hz.

694

695 *Electrophysiology in sedated monkeys*

696 Monkeys were sedated with a continuous intravenous infusion of propofol (5 ml/kg/h) that  
697 minimizes effects on spinal cord stimulation<sup>56</sup>. We delivered single pulses of cathodic, charge  
698 balanced, asymmetric square pulses (0.3 ms, 1 Hz) from each electrode contact while recording  
699 compound potentials from all implanted arm and hand muscles. Electromyographic signals were  
700 acquired with a Behavioral Neurophysiology chronic recording system (RZ2 BioAmp Processor,  
701 Tucker-Davis Technologies, USA) at a sampling frequency of 12207 Hz. We then delivered 10  
702 repetitions of pulse trains from each contact, at several frequencies ranging from 20 to 120 Hz.  
703 We recorded compound potentials from all implanted arm and hand muscles and arm kinematics  
704 through two high resolution cameras (Sony FDR-X3000 Action Cam 4K). Through this procedure  
705 we identified three contacts that primarily elicited (1) arm flexors, (2) arm extensors and (3) hand  
706 flexors. In a reduced set of trials, we also recorded the force produced by arm flexion through a  
707 10 N range force sensor (Dual-Range Force Sensor, DFS-BTA, Vernier, Beaverton, Oregon,  
708 USA). To record the pulling force produced during isometric arm flexion, the hand was fixated to  
709 the sensor hook through a string, and the sensor and the elbow were kept in place by two  
710 experimenters, to optimally capture the strength produced by muscle contraction.

711 *Behavioral experimental recordings*

712 All animals were trained to perform a three-dimensional robotic reach, grasp and pull task,  
713 previously described in detail in (Barra 2019<sup>41</sup>) and briefly recalled in the supplementary  
714 information.

715

716 For Mk-Sa, data presented in this paper were collected several weeks pre lesion and 1 week post  
717 lesion, unfortunately a severe infection of the spinal array and EMGs that recurred after day 7  
718 lead to the premature euthanasia of the monkey before the study could be completed, in  
719 agreement with the endpoints in our veterinary authorization. For Mk-Br and Mk-Yg data  
720 presented in this paper were collected several weeks pre lesion and until 3 weeks post lesion. At  
721 the end of week 3 post lesion, Mk-Br had 2 episodes of self-mutilation on the foot ipsi-lateral to  
722 the lesion. In consequence we euthanized the animal before the end of the protocol according to  
723 the endpoints in our veterinary authorization. As described in the results section, we found post-  
724 mortem that Mk-Br had a medial spinal cord contusion at the T3 level. While this lesion did not  
725 affect motor control of the legs or the arms, it may have generated neuropathic pain. Mk-Yg could  
726 perform the entire protocol without any adverse event, however after day 7, the caudal contact of  
727 the spinal interface (E8) identified to promote grasp failed, thus preventing us to perform  
728 experiments with optimal stimulation configuration and impacting the efficacy of grasp movements.

729

730

731 *Optimization of EES parameters*

732 To optimize stimulation parameters we exploited the frequency/kinematic relationship that we  
733 observed during single contact stimulation (**Figure 3B,E**). We then analyzed single joint  
734 movements at different frequencies and contacts and weighted joint excursion angles against  
735 movement smoothness<sup>57</sup>, we found that stimulation frequencies of 50-60 Hz (**Extended Data**  
736 **Figure 5**) produced smooth<sup>57</sup> and full-range movements and maximal forces. Instead, movements  
737 elicited at frequencies lower than 40 Hz were too weak to complete a full joint movement while  
738 frequencies higher than 60 Hz produced either abrupt movements or incomplete movements  
739 (**Extended Data Figure 5A**). Next, we identified among all the tested contacts, those that could  
740 consistently elicit arm extension (reach), hand flexion (grasp) and arm flexion (pull) (**Extended**  
741 **Data Figure 5B**). We chose these contacts and 50-60Hz to sustain full arm and hand movement  
742 and tested their effect in anesthetized animals by sequentially executing bursts on each of these  
743 three contacts. We verified that the sequence triggered whole arm and hand movements that  
744 mimicked smooth<sup>57</sup> and natural multi-joints movements (**Extended Data Figure 5C, Video 1**).  
745 Specifically, extension, grasping and pulling movements produced clear EMG bursts as well as  
746 robust and smooth kinematics. These stimulation protocols could be triggered by an operator at  
747 the beginning of each reach movement or automatically from intra-cortical signals in real-time.  
748 Therefore, we verified that movement onset could be detected from intra-cortical signals even  
749 after SCI (**Extended Data Figure 5**).  
750

751 *Stimulation during three-dimensional reach and pull task in injured monkeys*

752 All monkeys were recorded after injury as soon as they could independently move in their housing,  
753 feed themselves autonomously and did not show signs of discomfort. This corresponded to 3, 5  
754 and 6 days after injury respectively for Mk-Yg, Mk-Br and Mk-Sa. After injury, the animals were  
755 reluctant to perform the task which required intense manual activity by the trainers to encourage  
756 them with the use of special positive rewards. Moreover, in consequence of the arm and hand  
757 impairments animals were quickly exhausted. As a result, the output of consistent behavior/day  
758 was low, and we were able to collect robust data in about 1day/week per animal after SCI. Each  
759 session was organized as follows. First, we executed two blocks without stimulation, each of the  
760 duration of approximately 2 minutes. During those blocks we visually evaluated the impairment  
761 level of the animal and the performance of the brain decoder. Second, we used the brain decoder  
762 to trigger specific stimulation patterns. Contacts used to elicit those functions were defined  
763 through the experiments described in the previous paragraph and combined together to create  
764 stimulation protocols that allowed the animal to perform a full reach, grasp and pull movement.

765 *Identification and classification of arm movements for kinematic analysis*

766 We defined the movement performed by the animals as composed of three different phases:  
767 reach, grasp and pull. The identification of the reach phase was done by marking the moment in  
768 which the left hand left the metallic bar to when the hand closed around the object secured to the  
769 robot hand effector (the grasp event). The grasp phase was considered to be a window of 100  
770 ms around the moment in which hand closed around the object. The pull phase started from the  
771 grasp event and finished when the animal accomplished the task by pulling the object towards its  
772 body and placed the hand back on the resting bar. Events related to the 3 phases of the movement  
773 (movement onset: reaching, grasp onset: grasping and release of the object, and pulling) were  
774 identified manually by inspecting video recordings from Vicon Motion Systems (Oxford, UK).

775 Moreover, a blind experimenter manually inspected the same video recordings from Vicon Motion  
776 System to mark successful and complete performance of reach, grasp and pull movements as  
777 events. A successful reach was defined as a complete extension of the arm that brought the hand  
778 at the position of the target (even when grasp could not be performed). A successful grasp was  
779 defined as a successful closure of the hand around the target. A successful pull was defined as  
780 the accomplishment of a flexion movement that brought the target towards the animal. Events  
781 were then extracted from Vicon and used to perform analysis on the kinematic of the movements  
782 and to train the brain decoder by automatic routines (Matlab 2019b). All the analysis was  
783 conducted as blinded experiments.

784 *Decoding motor states from intracortical signals*

785 We designed a neural decoder that detected reaching and grasping events using intracortical  
786 spiking activity. To detect spikes, we set a threshold on each channel of -4 times the root-mean-  
787 square voltage recorded during a brief period while the monkey was at rest. We estimated firing  
788 rates in each of the motor cortical array channels by summing the multiunit spikes with a 150 ms  
789 history every 0.5 ms. We used these multiunit firing rate estimates to compute a twenty-  
790 dimensional neural manifold capturing the majority of population variance<sup>47</sup>. We projected the  
791 spiking activity onto this manifold to calibrate a multiclass regularized linear discriminant analysis  
792 decoder<sup>39</sup> that predicted the labeled timing of reach and grasp events. The decoder used 500 ms  
793 of past neural activity and output the probability of observing the reach and grasp events. During  
794 calibration, we defined a probability threshold for each event ranging from 0.8 to 0.99 to optimize  
795 predictions of the timing of each event using cross-validation. Since the monkeys could not  
796 complete the task after SCI, we were unable to consistently acquire labeled training data. We  
797 therefore calibrated a decoding algorithm using reaches from a recording session of a healthy  
798 monkey. We then manually labeled attempted reaches after SCI by manual inspection of video  
799 recordings. Using canonical correlation analysis, we aligned the neural dynamics<sup>58</sup> preceding  
800 reaches on the healthy sessions to the observed neural dynamics preceding attempted reaches  
801 after SCI. These aligned dynamics were used to control the decoder trained on the healthy  
802 reaches.

803 We implemented a custom C++ software application running a control suite that used the  
804 decoding algorithm to trigger EES stimulation in real-time. The application received neural data  
805 over UDP and made predictions using the decoding algorithm at 15 ms intervals. When the output  
806 probabilities crossed the defined threshold, the application triggered preprogrammed patterns of  
807 EES.

808 *Analysis of muscle recruitment curves*

809 Electromyographic activity was bandpass filtered between 30 and 800 Hz with an offline 3<sup>rd</sup> order  
810 Butterworth filter and stimulus artifact were removed. For each animal, stimulation contact, muscle  
811 and stimulation amplitude, we extracted compound potentials from 50ms-long segments of  
812 electromyographic activity following a stimulation pulse. We then computed the peak-to-peak  
813 amplitude of compound potentials. Since we gave four pulses of stimulation for each selected  
814 current amplitude, we averaged across values corresponding to the same stimulation amplitude  
815 and represented as the mean recruitment value of each muscle as a function of the injected  
816 current. For each muscle, recruitment values have been subsequently normalized by the  
817 maximum value obtained for that specific muscle, provided that we obtained response saturation  
818 (and therefore maximal contraction) in at least one occasion during the session. In addition, we

819 computed a selectivity index for each muscle<sup>59</sup>.

820 In order to obtain a comprehensive measure of muscle recruitment for each contact that would  
821 allow to compare across animals, we computed, for each animal, each muscle and each contact,  
822 an Average Recruitment Index (ARI) as the average of the recruitment values across all  
823 stimulation amplitudes used from a specific stimulation site.

824 To compute muscle recruitment during the delivery of pulse train stimulation, we computed the  
825 energy of the EMG signal during the duration of stimulation. We then applied the same  
826 normalization procedure described above for single pulse recruitment.

827 *Analysis of muscle activity during EES*

828 Electromyographic activity was bandpass filtered between 30 and 800 Hz with an offline 3<sup>rd</sup> order  
829 Butterworth filter and stimulus artifact were removed. In all animals we computed the energy EMG  
830 signals, for each implanted muscle. Energy of EMG signals during stimulation was computed on  
831 each segment in which stimulation was delivered after the animal started a movement attempt,  
832 with the formula here below:

833 
$$EN_{EMG} = \frac{1}{N} \sum_i^N \|EMG_i\|^2 dt$$

834 Where  $EMG_i$  is the value of EMG activity at sample  $i$ ,  $N$  is the number of samples in the signal  
835 and  $dt$  is the sampling resolution.

836 Energy of EMG signals without stimulation was computed on each segment in which stimulation  
837 was not delivered and the animal started a movement attempt. A movement attempt was defined  
838 as an increased EMG activity of the Biceps and Deltoid muscles.

839

840 *Analysis of task and kinematics performance*

841 We computed task performance as the rate of each movement expressed in events per minute.  
842 Successful movements were identified by a blind experimenter as movements performed skillfully  
843 and that had functional relevance (see above, *Identification and classification of arm movements*  
844 *for kinematic analysis*). First, we have identified all the sections of the recording during which the  
845 animal was actively attempting the task. All dead times, i.e. moments in which animals directed  
846 their attentions elsewhere than the task itself, were discarded from the analysis. Second, we  
847 computed the task performance frequency as the rate of successful movements per unit of time.  
848 In order to do this, we subdivided sessions in time bins of 1 second and we marked the presence  
849 or absence of successful trials, both with and without stimulation. We then used bootstrap to  
850 analyze significance of those results. Sessions when the animal did not perform the task were  
851 discarded from this analysis. Next, we performed Principal Component Analysis (PCA) on a large  
852 set of kinematic features. Details of this analysis are explained in the Supplementary information.

853

854 *Processing of cortical signals*

855 We identified spiking events on each channel when the band-pass filtered signal (250 Hz–5kHz)  
856 exceeded 3.0–3.5 times its root-mean-square value calculated over a period of 5s. We removed  
857 artifacts by deleting all the spikes that synchronously in at least 30 channels. We computed the  
858 firing rate of each channel as the number of spikes detected over non-overlapping bins of 10ms.  
859 Whenever we showed average firing rate activity, we sorted channels in order of activation in one  
860 reference trial, and subsequently applied the same ordering method to all other trials. Finally, we  
861 normalized the activity of each channel by its maximum firing rate.

862 *Comparison of motor cortical activity during EES evoking movement and no movement*

863 To study how motor cortical activity interacted with EES, we analyzed the neural recordings from  
864 Mk-Br and Mk-Yg. We identified periods where EES pulse trains produced no discernible  
865 movements by setting a threshold on hand velocity. We compared multi-unit neural firing rates on  
866 each channel in this period to neural firing rates in the previously identified trials where EES  
867 enabled reaching and grasping. First, we counted the number of spikes within the window of  
868 stimulation and divided by the duration of stimulation. We then averaged across stimulus  
869 repetitions of the movement and no movement conditions and pooled across recording sites in  
870 motor cortex.

871 We next computed instantaneous estimates of multi-unit firing rates on each channel by counting  
872 the number of spikes in non-overlapping 20 ms bins and convolving with a gaussian kernel of 50  
873 ms width. We applied Principal Component Analysis (PCA) to compute 10-dimensional neural  
874 manifolds spanning this multi-unit population activity<sup>47</sup>. We projected the neural activity onto these  
875 manifold axes during the periods where EES evoked either movement or no movement. We then  
876 identified periods where the monkey was at rest with no EES, as well as periods where the  
877 monkey attempted movements of the arm with no EES. To compare the similarity of neural activity  
878 between these conditions, we computed the Mahalanobis distance between activity at rest and  
879 the three other periods: EES with movement, EES with no movement, and attempted movements  
880 with no EES.

881 *Histology*

882 Monkeys were deeply anesthetized (lethal dose of pentobarbital, 60mg/kg, injected i.v.) and  
883 transcardially perfused with saline (about 200 ml), followed by 3 liters of 4% paraformaldehyde  
884 (PFA). Dissected spinal cord were post-fixed in 4% PFA overnight, and then immersed in 30%  
885 sucrose solution for 2 weeks. 50µm transverse or horizontal sections were cut using a cryostat  
886 and kept in 0.1M PBS azide (0.03%) at 4°C. Primary antibodies were: rabbit anti-Iba1 (1:1000,  
887 Wako) and guinea pig anti-NeuN (1:300, Millipore). Fluorescence secondary antibodies were  
888 conjugated to: Alexa fluor 647 (1:200, Life technologies) and Alexa fluor 555 (1:300, Life  
889 technologies). Sections were coverslipped using Mowiol. Immunofluorescence was imaged  
890 digitally using a slide scanner (Olympus VS-120). Lesions were reconstructed using image  
891 analysis software (Neurolucida) to trace the lesion over serial sections (200 µm apart).

892 *Statistical procedures*

893 All data are reported as mean values ± standard error of the mean (s.e.m.) or mean values ±  
894 standard deviation (std). The choice is highlighted directly in the figures or in the relative  
895 caption. Significance was analyzed using the non-parametric Wilcoxon rank-sum test. In the  
896 comparisons shown in Figure 3 we subsequently applied the Bonferroni correction. In only one

897 case (Figure 4A, 4B), significance was analyzed using bootstrap. The level of significance was  
898 set at \* $p<0.05$ , \*\* $p<0.01$ , \*\*\* $p<0.001$ .  
899 No statistical methods were used to pre-determine sample sizes instead number of animals used  
900 in this study are consistent to other works that involved similar procedures in monkeys<sup>9,10,42</sup>.  
901

## 902 **Data availability**

903 Due to the sensitive nature of the dataset, which contains graphic information on monkeys, raw  
904 data, including videos, will be available upon reasonable request to the corresponding author and  
905 after authorization from the Swiss cantonal authorities. A set of pre-processed data will be  
906 deposited on the open-data commons for spinal cord injury (<https://odc-sci.org>).  
907

## 908 **Code availability**

909 Software routines utilized for data analysis will be deposited on GitHub under search keyword  
910 NN-A75365C.  
911

## 912 **METHODS REFERENCES**

- 913 54. National Research Council (US) Institute for Laboratory Animal Research. *Guide for*  
914 *the Care and Use of Laboratory Animals*. (National Academies Press (US), 1996).
- 915 55. Mathis, A. et al. DeepLabCut: markerless pose estimation of user-defined body parts  
916 with deep learning. *Nature neuroscience* **21**, 1281–1289 (2018).
- 917 56. Toossi, A. et al. Effect of anesthesia on motor responses evoked by spinal neural  
918 prostheses during intraoperative procedures. *Journal of neural engineering* **16**,  
919 036003 (2019).
- 920 57. Teulings, H.-L., Contreras-Vidal, J. L., Stelmach, G. E. & Adler, C. H. Parkinsonism  
921 Reduces Coordination of Fingers, Wrist, and Arm in Fine Motor Control.  
922 *Experimental Neurology* **146**, 159–170 (1997).
- 923 58. Gallego, J. A., Perich, M. G., Chowdhury, R. H., Solla, S. A. & Miller, L. E. Long-term  
924 stability of cortical population dynamics underlying consistent behavior. *Nature*  
925 *neuroscience* **23**, 260–270 (2020).
- 926 59. Raspopovic, S., Capogrosso, M. & Micera, S. A Computational Model for the  
927 Stimulation of Rat Sciatic Nerve Using a Transverse Intrafascicular Multichannel  
928 Electrode. *IEEE Transactions on Neural Systems and Rehabilitation Engineering* **19**,  
929 333–344 (2011)

930

931